The germline coordinates mitokine signaling

Authors: Koning Shen[1], Jenni Durieux[1,2], Cesar G. Mena[1,2,3], Brant M. Webster[1,4], C. Kimberly Tsui[1], Hanlin Zhang[1], Lawrence Joe[1,2], Kristen Berendzen[5], and Andrew Dillin[1,2,6*].

Affiliations:
[1]Department of Molecular & Cellular Biology, University of California, Berkeley, Berkeley CA 94720, USA.
[2]Howard Hughes Medical Institute, University of California, Berkeley, Berkeley CA 94720, USA.
[3]Present affiliation: Stanford University, Palo Alto, CA 94305, USA.
[4]Present affiliation: Denali Therapeutics, South San Francisco, CA 94080, USA.
[5]Weill Institute for Neurosciences, University of California, San Francisco, San Francisco CA 94118, USA.
[6]The Helen Wills Neuroscience Institute, University of California, Berkeley, Berkeley CA 94720, USA.

*Corresponding author: dillin@berkeley.edu

Abstract

The ability of mitochondria to coordinate stress responses across tissues is critical for health. In *C. elegans*, neurons experiencing mitochondrial stress elicit an inter-tissue signaling pathway through the release of mitokine signals, such as serotonin or the WNT ligand EGL-20, which activate the mitochondrial unfolded protein response (UPR^{MT}) in the periphery to promote organismal health and lifespan. We find that germline mitochondria play a surprising role in neuron-to-peripheral UPR^{MT} signaling. Specifically, we find that germline mitochondria signal downstream of neuronal mitokines, like WNT and serotonin, and upstream of lipid metabolic pathways in the periphery to regulate UPR^{MT} activation. We also find that the germline tissue itself is essential in UPR^{MT} signaling. We propose that the germline has a central signaling role in coordinating mitochondrial stress responses across tissues, and germline mitochondria play a defining role in this coordination because of their inherent roles in germline integrity and inter-tissue signaling.

Introduction

Multi-cellular organisms must coordinate the health and function of varied tissues across the organism in order to maintain overall health. This has led to the development of specialized tissues or organs that can communicate long-range signaling with other tissues to ensure organismal health. For instance, the central nervous system regulates the activity of other organs in the body through hormones or neuronal signaling (e.g. neurotransmitters and neuropeptides). Similarly, muscle or adipose fat can send metabolic or hormonal signals to other components of the body under conditions of hunger, overnutrition, or exercise.

These pathways of inter-tissue signaling become especially crucial during conditions of stress, such as pathogenic infection or cold exposure (Castillo-Armengol et al., 2019; Rao et al., 2017), or during unhealthy aging, where the aging-induced dysfunction in certain organs may contribute to loss of inter-tissue communication pathways and a broader loss of organismal health (Smith et al., 2020; Van Oosten-Hawle, 2023). For instance, over-accumulation of inflammation or senescent cells in certain tissues, such as muscle and the brain, can release blood-borne factors that affect the aging process (Bieri et al., 2023; Horowitz et al., 2020). In some cases, these secreted factors are protective, such as GDF11 which increases synaptic plasticity and neurogenesis (Bieri et al., 2023; Katsimpardi et al., 2014; Ozek et al., 2018). However, some secreted factors can also aggravate the aging process, such as the proinflammatory chemokines secreted by senescent cells (Birch and Gil, 2020), suggesting that inter-tissue signaling mechanisms must be tightly regulated to ensure organismal health.

Signals for inter-tissue communication can arise from a multitude of cellular sources, and mitochondria are a prominent source of these signals (Chandel, 2014; Mottis et al., 2019; Shen et al., 2022). This important signaling role for mitochondria may have arisen out of their

56 endosymbiotic origin. When the prokaryotic mitochondrial precursor was engulfed by its now-
57 eukaryotic host, the mitochondria had to develop comprehensive signaling pathways to
58 communicate with its new host cell and nuclear genome. Fittingly, these mitochondrial signaling
59 pathways are highly conserved and have been observed in species ranging from mammals through
60 invertebrates. In particular, mitochondria experiencing dysfunction use inter-tissue signaling
61 pathways to communicate their stress to other tissues and activate protective cellular programs,
62 such as the mitochondrial unfolded protein response (UPR^{MT}), a transcriptional program activated
63 under conditions of mitochondrial stress to alleviate mitochondrial burden and promote overall
64 cellular and organismal health (Houtkooper et al., 2013; Moehle et al., 2019; Shpilka and Haynes,
65 2018). In mice, low-level mitochondrial stress in POMC neurons induced by *Crif1*
66 heterodeficiency signals to white adipose tissue to increase thermogenesis and activate the UPR^{MT}
67 to protect against obesity and enhance metabolic turnover (Kang et al., 2021). In *Drosophila*,
68 muscle tissue experiencing mild mitochondrial stress also activates the UPR^{MT} and induces
69 expression of ImpL2 (an ortholog to the human insulin-like growth factor binding protein IGFBP7)
70 that suppresses whole-organism insulin signaling, upregulates mitophagy, and promotes longevity
71 and muscle function (Owusu-Ansah et al., 2013).

72 Much of the mechanistic work investigating inter-tissue mitochondrial signaling has been
73 performed in *C. elegans* using a model of inter-tissue (or cell nonautonomous) communication of
74 the UPR^{MT} between neurons and the intestine (Durieux et al., 2011). In this model, neurons
75 experiencing mitochondrial stress, such as neuron-specific knockdown of mitochondrial genes
76 (Durieux et al., 2011), expression of the aggregation-prone mutant PolyQ40 protein, or neuron-
77 specific targeting of KillerRed to mitochondria (Berendzen et al., 2016), activate the UPR^{MT} in the
78 intestine, a tissue in *C. elegans* completely peripheral and non-innervated by neurons **(Fig 1A)**.

79 Intestinal activation of UPR^{MT} by these neurons protected organismal health, as inhibition of
80 UPR^{MT} activation decreased organismal fitness in the presence of neuronal mitochondrial stress
81 (Berendzen et al., 2016).

82 Several neuronal factors mediating neuron-to-intestine UPR^{MT} signaling in *C. elegans* have
83 been identified. Neuron-specific over-expression of the histone demethylases *jmjd-1.2* and *jmjd-*
84 *3.1* induces intestinal UPR^{MT} even in the absence of mitochondrial stress and also regulates
85 activation of UPR^{MT} in mice (Merkwirth et al., 2016). Neuronal release of neurotransmitters like
86 serotonin or the neuropeptides FLP-1 and FLP-2 are also critical in mediating cell nonautonomous
87 activation of the UPR^{MT} and other stress responses in the intestine (Berendzen et al., 2016; Jia and
88 Sieburth, 2021; Shao et al., 2016). The WNT ligand, EGL-20, was identified as a bona fide
89 "mitokine" as it is both necessary and sufficient for activation of the intestinal UPR^{MT} upon
90 neuron-specific over-expression (Zhang et al., 2018). Neuronal release of the EGL-20 WNT ligand
91 engages canonical WNT signaling pathway in the peripheral intestinal cells to activate the UPR^{MT}
92 (Zhang et al., 2018). However, a dichotomy exists because the canonical developmental program
93 regulated by WNT signaling is not subsequently induced. Therefore, how this WNT signaling, in
94 the context of neuronal mitochondrial stress, could specifically induce the UPR^{MT} and not its
95 canonical developmental programs in the intestine is unknown.

96 To address this question, we performed a genome-wide mutagenesis screen in *C. elegans*
97 to identify molecular players that mediated UPR^{MT} cell nonautonomous signaling between neurons
98 and the intestine. Through this screen, we identified mutations in the *ucr-2.3* gene that are essential
99 in mediating cell nonautonomous UPR^{MT} signaling between neurons and the intestine. *ucr-2.3* is
100 a mitochondrial electron transport chain (ETC) complex III gene, homologous to mammalian
101 UQCRC2, and is expressed primarily in a few neurons and the germline of *C. elegans*. Surprisingly,

102 we discovered that germline activity, not neuronal, of *ucr-2.3* mediates the cell nonautonomous
103 UPR^{MT} signaling between the neurons and intestine. In addition, we find that the germline plays a
104 general role in mediating cell nonautonomous UPR^{MT} signaling, as loss of the germline through
105 either genetic or pharmacological treatments abolishes neuron-to-intestine UPR^{MT} activation, but
106 not other neuronal derived stress signals. These data suggest that integrity of the germline tissue,
107 mediated through germline UCR-2.3 mitochondrial activity, is integral for neuron-to-intestinal
108 signaling of the UPR^{MT}. Finally, we find that germline integrity may regulate intestinal UPR^{MT}
109 activation through altering lipid metabolism and transport pathways between reproductive and
110 intestine tissues. Overall, our work showcases a signaling role for the germline, once thought of
111 as a tissue insulated from the soma, in directly communicating with somatic tissues for stress
112 signaling. Additionally, our results provide broader implications for the importance of germline
113 mitochondrial quality and its physiological interactions with neuronal signaling and intestinal lipid
114 metabolism, and the consequences of these interactions on organismal stress signaling and fertility.
115

116 **Results**

117 **Mutagenesis screen reveals the requirement of *ucr-2.3* in neuronal UPR^{MT} signaling**

118 To identify novel regulators of inter-tissue (or cell nonautonomous) mitochondrial
119 signaling in *C. elegans*, we conducted a genome-wide mutagenesis screen using a genetic model
120 where neurons expressing an aggregation-prone mutant PolyQ40 protein tagged with YFP (*rgef-*
121 *1p::Q40::*YFP) activates the mitochondrial unfolded protein response (UPR^{MT}) in the intestine
122 (Berendzen et al., 2016) **(Fig 1A)**. Activation of the UPR^{MT} in the intestine can be assessed by a
123 transcriptional reporter for expression of *hsp-6*, the mitochondrial Hsp70 chaperone induced by
124 the UPR^{MT} (Shpilka and Haynes, 2018) **(Fig 1A)**. After identifying mutants with suppressed

125 intestinal UPR^{MT} but intact neuronal PolyQ40 signal, we used SNP mapping and whole genome
126 sequencing approaches (Doitsidou et al., 2010) to identify one causative mutation that suppressed
127 cell nonautonomous UPR^{MT} signaling as a missense mutation in the gene *ucr-2.3* **(Supp Fig 1A,**
128 **F)**. We independently verified the necessity of *ucr-2.3* in mediating cell nonautonomous UPR^{MT}
129 signaling by creating several alleles of early stop codon, nonsense-mediated decay (NMD)
130 mutations in *ucr-2.3* through CRISPR/Cas9 genome editing and observed that they all suppressed
131 PolyQ40-mediated cell nonautonomous UPR^{MT} **(Fig 1B; Supp Fig 1B, F)**. Importantly, the NMD
132 early stop codon mutation in the *ucr-2.3(uth252)* allele leads to almost complete loss of gene
133 expression, thus effectively creating a null allele **(Supp Fig 1D, F)**. We also tested a *ucr-2.3* mutant
134 containing a large deletion spanning exons 3-4 resulting in an early termination codon and found
135 that it also suppressed cell nonautonomous UPR^{MT} signaling **(Supp Fig 1C, F).** We also tested
136 whether *ucr-2.3* was involved in other models of cell nonautonomous UPR^{MT} signaling, such as
137 neuron-specific knockdown of the mitochondrial complex IV subunit *cco-1* (*rab-3p::cco-1* hairpin
138 in the *sid-1(qt9)* genetic background), which also activates UPR^{MT} in the intestine (Durieux et al.,
139 2011). We find that a null mutation in *ucr-2.3* also suppresses this model of cell nonautonomous
140 UPR^{MT} signaling **(Fig 1C)**. Therefore, we conclude that *ucr-2.3* is as a novel regulator of neuron-
141 to-intestine UPR^{MT} signaling induced by multiple forms of neuronal mitochondrial stress.

142 Next, we tested whether *ucr-2.3* was required for cell autonomous induction of the UPR^{MT}.
143 We tested this by feeding *cco-1* RNAi targeting a mitochondrial complex IV subunit to wildtype
144 and *ucr-2.3* mutant strains to ask whether loss of *ucr-2.3* impairs cell-autonomous activation of
145 the UPR^{MT}. We find that *ucr-2.3* loss of function mutants still activate, not inhibit, the UPR^{MT} cell
146 autonomously, with and without neuronal PolyQ40 expression **(Fig 1D, Supp Fig 1E)**. These data
147 indicate that *ucr-2.3* is not involved in general machinery of UPR^{MT} activation but rather has a

148 specific role in cell nonautonomous signaling of mitochondrial stress. We also find that loss of
149 *ucr-2.3* non-autonomous UPR^{MT} signaling is not a temporary delay. Rather, the suppression of
150 non-autonomous UPR^{MT} signaling by the *ucr-2.3* mutation increases over aging **(Supp Fig 1G)**.
151 Finally, we tested the specificity of *ucr-2.3* loss in nonautonomous stress signaling and find that
152 *ucr-2.3* loss of function does not suppress cell nonautonomous signaling of the UPR^{ER} or the
153 cytosolic heat stress response (HSR) between neurons and the intestine **(Supp Fig 2A-B)**.
154 Conversely, there is a slight up-regulation of both stress responses upon *ucr-2.3* loss of function.
155 Overall, our data indicate that *ucr-2.3* is a critical and specific gene required for mediating cell
156 nonautonomous UPR^{MT} signaling between neurons and the intestine in *C. elegans*.
157

158 **UCR-2.3 is a mitochondrial protein with a novel role in mitochondrial stress signaling**

159 The *ucr-2.3* gene encodes UCR-2.3 in *C. elegans*, which is reported to be a mitochondrial
160 protein homologous to mammalian UQCRC2, a core subunit of respiratory complex III of the
161 electron transport chain (Iwata et al., 1998; Nomura et al., 2006). That the loss of *ucr-2.3* results
162 in a loss of UPR^{MT} neuronal signaling was perplexing because the knockdown of many
163 mitochondrial proteins, especially those involved in the electron transport chain, activate, not
164 suppress, the UPR^{MT} (Durieux et al., 2011; Houtkooper et al., 2013; Nargund et al., 2012). Indeed,
165 we observed that even in "basal" conditions, i.e. no additional source of stress, the *ucr-2.3* null
166 mutation still does not activate UPR^{MT} **(Supp Fig 2C)**, suggesting that UCR-2.3 in mitochondria
167 may have a non-canonical role in regulating UPR^{MT} signaling.

168 We experimentally confirmed that the UCR-2.3 protein is a mitochondrial protein using
169 three orthogonal approaches. First, we performed a sub-cellular fractionation in *C. elegans*
170 expressing *ucr-2.3* with an HA epitope endogenously inserted at the *ucr-2.3* genomic locus using

171 CRISPR/Cas9 editing **(Fig 2A*i*)**. Compared to the cytosolic fraction, we detected enrichment of
172 UCR-2.3 in the mitochondrial fraction similar to that of NDUFS3, a subunit of mitochondrial
173 electron transport complex I, and as opposed to α-tubulin, which was detected predominantly in
174 the cytosolic fraction **(Fig 2A*ii*)**. Second, using human RPE-1 cells, we over-expressed the *C.*
175 *elegans* UCR-2.3 protein tagged with mNeonGreen alongside an outer mitochondrial membrane
176 protein OMP25 tagged with BFP **(Fig 2B)**. We find that UCR-2.3 and OMP-25 thoroughly co-
177 localize (mean 71.8%, SD = 18.2%), indicating the UCR-2.3 is highly localized to mitochondria
178 **(Fig 2B*i*)**. Indeed, upon closer examination, we observed that UCR-2.3 primarily localizes within
179 the OMP25 signal, suggesting that UCR-2.3 is located within the mitochondrial matrix, consistent
180 with its purported role as a matrix-facing core subunit of complex III like UQCRC2 **(Fig 2B*ii*)**
181 (Iwata et al., 1998). Third, we observed that UCR-2.3 functionally acted as a mitochondrial protein.
182 Using the null mutation in *ucr-2.3* in *C. elegans*, we observed that loss of *ucr-2.3* decreased
183 mitochondrial respiration **(Fig 2C)**. Thus, we conclude that *ucr-2.3* encodes a bona fide
184 mitochondrial protein in *C. elegans*, which has a similar sub-cellular localization and function to
185 its mammalian ortholog UQCRC2.

186 Next, we tested whether UCR-2.3 mitochondrial localization was essential for its role in
187 mediating cell nonautonomous UPR^{MT} signaling. Using CRISPR/Cas9 genomic editing, we
188 excised the predicted mitochondrial targeting sequence (MTS) of UCR-2.3 predicted by MitoFates
189 (Fukasawa et al., 2015) from UCR-2.3 and found that this ΔMTS mutation *ucr-2.3(ΔMTS)*
190 suppressed intestinal UPR^{MT} signaling **(Fig 2D)** but had no effect on *ucr-2.3* expression **(Supp**
191 **Fig 2D)**. Overall, we conclude that *ucr-2.3* encodes a mitochondrial localized protein whose
192 mitochondrial activity is important for regulating neuron-to-intestine cell nonautonomous UPR^{MT}
193 signaling in a manner atypical of canonical mitochondrial electron transport chain proteins.

194

195 ***ucr-2.3* has a unique role within the UCR-2 gene family in *C. elegans***

196 *ucr-2.3* belongs to a family of paralogs in the UCR-2 family in *C. elegans* that are all
197 homologous to mammalian UQCRC2: *ucr-2.1, ucr-2.2,* and *ucr-2.3* **(Fig 3A)** (Howe et al., 2016).
198 To investigate whether the other paralogs of the UCR-2 family were also involved in cell
199 nonautonomous UPR^{MT} signaling, we made similar early stop codon NMD mutations in *ucr-2.1*
200 and *ucr-2.2* using CRISPR/Cas9 editing **(Supp Fig 3E*i-ii*)**. Surprisingly, we found that only
201 genetic loss of *ucr-2.3* suppressed cell nonautonomous UPR^{MT} signaling **(Fig 3B)**. Genetic loss of
202 *ucr-2.1* or *ucr-2.2* slightly activated, not suppressed, UPR^{MT}, more in alignment with the
203 expectation of a canonical mitochondrial gene knockdown **(Fig 3B)**. This suggested that *ucr-2.3*
204 has a unique role among the UCR-2 family genes, whereas *ucr-2.1* and *ucr-2.2* may be more
205 similar and typical of electron transport chain subunits.

206 Next, we next sought to explore the functional and genetic relationships among the UCR-
207 2 family genes. First, we observed that *ucr-2.1* and *ucr-2.2* were functionally redundant with each
208 other with respect to their role in the mitochondrial electron transport chain, but neither were
209 redundant with *ucr-2.3.* While knockdown of *ucr-2.3* reduced mitochondrial respiration **(Fig 2C)**,
210 only the double knockdown of *ucr-2.1* and *ucr-2.2* could reduce mitochondrial respiration **(Supp**
211 **Fig 3A)**. Individual knockdown of either *ucr-2.1* or *ucr-2.2* had no effect on respiration, suggesting
212 that these two genes are functionally redundant with each other **(Supp Fig 3A)**. In addition, double
213 knockdown of *ucr-2.1* and *ucr-2.2* strongly activated UPR^{MT}, while the single knockdowns had no
214 effect **(Supp Fig 3B)**. As this strong activation is consistent with the expectation of a canonical
215 mitochondrial ETC gene knockdown (Durieux et al., 2011; Houtkooper et al., 2013), this provides
216 further evidence that *ucr-2.1* and *ucr-2.2* are functionally redundant with each other for a role in

217 the mitochondrial electron transport chain, likely together recapitulating the role of the mammalian
218 UQCRC2 complex III subunit. In contrast, we observed that double knockdown of either *ucr-2.1*
219 and *ucr-2.3* or *ucr-2.2* and *ucr-2.3* could not activate UPR^{MT}; only conditions in which both *ucr-*
220 *2.1* and *ucr-2.2* are knocked down could UPR^{MT} be activated **(Supp Fig 3C)**. This finding further
221 suggests that neither *ucr-2.1* nor *ucr-2.2* are functionally redundant with *ucr-2.3.*

222 In addition, we analyzed how knockdown of these UCR-2 family genes affected each other
223 transcriptionally. We found that while knockdown of *ucr-2.3* increased expression of *ucr-2.1* and
224 *ucr-2.2* **(Supp Fig 3D)**, knockdown of either *ucr-2.1* or *ucr-2.2* individually or together had no
225 effect on *ucr-2.3* expression **(Supp Fig 3E)**. One interpretation of this result is that loss of *ucr-2.3*
226 function requires compensation from both *ucr-2.1* and *ucr-2.2* equally, while loss of either *ucr-2.1*
227 or *ucr-2.2* does not require *ucr-2.3.* Altogether, these data suggest that *ucr-2.1* and *ucr-2.2* are
228 functionally redundant with each other while *ucr-2.3* may have an independent role.

229 Most importantly, we found that the UCR-2 family genes differ in their tissue expression
230 patterns **(Fig 3C-D)**. Using genomic, tissue-specific, and single cell transcriptomic databases, we
231 found that while *ucr-2.1* and *ucr-2.2* expression is mostly ubiquitous through the animal, *ucr-2.3*
232 expression is enriched in the germline and neuronal cells (Cao et al., 2017; Howe et al., 2016;
233 Kaletsky et al., 2018) **(Supp Fig 3F)**. We confirmed these reports by generating an endogenous
234 transcriptional expression reporter system for each of the UCR-2 genes by inserting an
235 mCherry::F2A construct between the promoters of *ucr-2.1*, *ucr-2.2*, and *ucr-2.3* and the respective
236 CDS at the endogenous genomic loci using CRISPR/Cas9 editing **(Fig 3C)**. The tissue expression
237 patterns confirm that *ucr-2.1* and *ucr-2.2* are mostly ubiquitously expressed throughout the somatic
238 tissues of the animal, though largely excluded from the germline **(Fig 3C*i-ii*, 3D)**. In contrast, *ucr-*
239 *2.3* expression was exclusively localized to the germline as well as a few cells in the head of the

240 animal **(Fig 3C*iii*, 3D)**. To determine which of these head cells expressed *ucr-2.3*, we crossed the
241 *ucr-2.3* expression reporter strain to an *rgef-1p::GFP* construct driving GFP expression in neurons
242 and found that the pattern of *ucr-2.3* expression mostly overlapped with the GFP signal **(Fig 3E)**,
243 suggesting that the cells expressing *ucr-2.3* are indeed neurons. In summary, our data indicate that
244 *ucr-2.3* differs starkly in its tissue expression from *ucr-2.1* and *ucr-2.2*, which may explain the
245 unique role of *ucr-2.3* in mediating cell nonautonomous UPR^{MT} signaling.
246
247 **The germline role of *ucr-2.3* is critical for mediating nonautonomous UPR^{MT}**
248 We were intrigued by the tissue-specific expression patterns of *ucr-2.3* and tested whether
249 this tissue-specific nature conferred the ability of *ucr-2.3* to mediate cell nonautonomous UPR^{MT}
250 signaling. To do this, we sought to determine the site of action for *ucr-2.3* for its role in cell
251 nonautonomous UPR^{MT} signaling. We designed a tissue-specific rescue experiment using the
252 single copy mosSCI system (Frøkjær-Jensen et al., 2008) **(Fig 4A)**. Briefly, we knocked in an
253 integrated wildtype copy of *ucr-2.3* driven by a tissue-specific promoter into a mutant strain of
254 *ucr-2.3*. As we observed that *ucr-2.3* is expressed in neuronal cells and the germline **(Fig 3C-D)**,
255 we tested whether either neuronal or germline-specific expression of wildtype *ucr-2.3* could rescue
256 cell nonautonomous UPR^{MT} signaling in the *ucr-2.3* mutant, using the neuron-specific promoter
257 *rgef-1* and the germline-specific promoter *pie-1* **(Fig 4A)**. We found that expression of a wildtype
258 copy of *ucr-2.3* driven by the germline-specific promoter *pie-1* could completely rescue the cell
259 nonautonomous UPR^{MT} signal suppressed by loss of *ucr-2.3*, whereas *rgef-1p* neuronal-driven
260 expression of *ucr-2.3* had no appreciable effect on cell nonautonomous UPR^{MT} signal **(Fig 4B)**. In
261 addition, one of our initial observations of the *ucr-2.3* mutants was their reduced brood size
262 (number of progeny) **(Fig 4C)**. We found that germline rescue of *ucr-2.3* could also completely

263 restore the brood size phenotype we observed with *ucr-2.3* mutants, whereas neuronal rescue of
264 *ucr-2.3* had no effect on the brood size **(Fig 4C)**.

265 We also used the FLP/FRT recombinase system to test how a neuron-specific knockout of
266 *ucr-2.3* affected nonautonomous UPR^{MT} signaling (Muñoz-Jiménez et al., 2017). We were unable
267 to use this system to test germline-specific knockout because germline-specific FLP/FRT
268 recombination becomes pervasive in all tissues in the following generation (Macías-León and
269 Askjaer, 2018). To design a neuron-specific FLP/FRT recombinase knockout system, we used the
270 *rgef-1p* neuronal promoter to drive FLP recombinase expression and inserted FRT sites in the
271 introns of *ucr-2.3* at the genomic locus. In this way, FLP recombination of *ucr-2.3* induced a large
272 deletion in the *ucr-2.3* genomic locus only in neuronal cells, which we confirmed by PCR
273 genotyping **(Supp Fig 4A*iii*)**. While *ucr-2.3* containing FRT sites had slightly reduced cell
274 nonautonomous UPR^{MT} signal, we find that FLP induced recombination of *ucr-2.3* did not enhance
275 reduction of the cell nonautonomous UPR^{MT} signal and did not phenocopy the loss of function
276 *ucr-2.3* genetic mutant **(Supp Fig 4A*i-ii*)**. Overall, these data identify that *ucr-2.3* mediates cell
277 nonautonomous UPR^{MT} signaling through its activity in the germline tissue.

278 Having previously discovered a role for *ucr-2.3* in mitochondrial respiration **(Fig 2C)**, we
279 next asked how much of the *ucr-2.3* mitochondrial activity is confined to the germline tissue. We
280 tested this by using a *C. elegans* strain with a temperature sensitive mutation in the *glp-4* gene,
281 which arrests germ cell proliferation at the restrictive temperature, 25 °C, to create germline
282 deficient adult animals (Beanan and Strome, 1992). We find that at the restrictive temperature 25
283 °C, *ucr-2.*3 loss of function still decreases mitochondrial respiration **(Fig 4D)**. Thus, germline
284 deficient animals also have decreased mitochondrial respiration, likely due to the loss of the high
285 population of mitochondria in the germline **(Fig 4D)** (Tsang and Lemire, 2002). However,

286 additional loss of *ucr-2.3* function in the germline deficient animals had no impact on
287 mitochondrial oxygen consumption **(Fig 4D)**. In contrast, feeding germline deficient animals with
288 a RNAi targeting the *cco-1* complex IV ETC subunit could further decrease mitochondrial
289 respiration **(Fig 4D)**. This indicates that the vast majority of *ucr-2.3* contribution to mitochondrial
290 respiration is in the germline.

291 In addition, we find that loss of *ucr-2.3* greatly changes morphology and content of
292 germline mitochondria. Using a germline-specific mitochondrial morphology reporter strain
293 (Ahier et al., 2018), we observe that wildtype animals have a dense network of mitochondria
294 throughout the germline tissue **(Fig 4E)**. However, the *ucr-2.3* mutation results in a more punctate
295 and sparser mitochondrial network in the distal germ cells and especially oocytes **(Fig 4E)**. In
296 addition, we find that while the average mitochondrial number (or mitochondrial density)
297 decreases in the *ucr-2.3* mutant **(Fig 4E*iii*)**, average mitochondrial length increases **(Fig 4E*iii*)**.
298 This result aligns with the idea that damaged mitochondria fuse together as compensation to
299 increase overall oxidative capacity (Youle and Van Der Bliek, 2012), as *ucr-2.3* loss of function
300 animals have compromised ETC activity **(Fig 2C, Fig 4D)**. Therefore, loss of *ucr-2.3* directly
301 affects the quality of germline mitochondria, and that loss of this germline mitochondrial quality
302 may compromise cell nonautonomous UPR^{MT} signaling.

303 Finally, we were intrigued by the germline tissue-specificity of *ucr-2.3* expression, as
304 compared to its paralogs *ucr-2.1* and *ucr-2.2* or other mitochondrial ETC proteins. We asked
305 whether nonautonomous UPR^{MT} signaling specifically required *ucr-2.3* activity or germline
306 mitochondrial quality more generally. To answer this, we first tested whether germline-specific
307 expression of the other *ucr-2* family genes, such as *ucr-2.1*, could rescue the *ucr-2.3* mutant
308 suppression of nonautonomous UPR^{MT}. Using the same single copy mosSCI system, we knocked

309 in an integrated wildtype copy of *ucr-2.1* driven by the *pie-1* germline-specific promoter into a
310 mutant strain of *ucr-2.3* **(Fig 4F)**. Surprisingly, we observed that germline-specific expression of
311 *ucr-2.1* could also rescue nonautonomous UPR^{MT} signaling in the *ucr-2.3* loss of function mutant.
312 Given the high sequence similarity between these two genes and their proposed similar function
313 in complex III of the electron transport chain as the UQCRC2 *C. elegans* homolog (Nomura et al.,
314 2006), this result suggests that general mitochondrial quality in the germline is essential for
315 nonautonomous UPR^{MT} signaling.

316 As an additional measure of germline mitochondrial quality, we asked whether knockdown
317 of mitochondrial genes that shared comparable tissue-specific paralogs as *ucr-2.3* could
318 recapitulate the UPR^{MT} suppression we observed with *ucr-2.3* mutants. Through searching the
319 same genomic and transcriptomic databases, we identified other mitochondrial electron transport
320 chain subunits that had similarly predicted patterns of gene expression in which one paralog was
321 ubiquitously expressed and another paralog was found restricted to neuronal and/or germline
322 expression. One such pairing we found was the complex I subunit gene *gas-1/nduf-2.1*
323 (ubiquitously expressed) and its related paralog *nduf-2.2* (neuron/germline expressed) **(Supp Fig**
324 **4B)** (Cao et al., 2017; Howe et al., 2016; Kaletsky et al., 2018). Similar to *ucr-2.3*, we used
325 CRISPR/Cas9 genetic engineering to create early stop codon NMD mutations in the *nduf-2.2*
326 genomic locus in the *rgef-1p::Q40::YFP; hsp-6p::GFP* genetic background. We observed that
327 early stop NMD mutation in *nduf-2.2* also suppressed cell nonautonomous UPR^{MT} signaling but
328 had no affect on autonomous UPR^{MT} signaling **(Fig 4G, Supp Fig 4C)**, similar to what we had
329 observed for *ucr-2.3* mutations **(Fig 1B, Supp Fig 1E)**. Therefore, general germline mitochondrial
330 dysfunction inhibits neuronal derived cell nonautonomous UPR^{MT} signaling.
331

332 **The germline, and germline mitochondria, is required for cell nonautonomous UPR^{MT}**
333 **signaling**

334 Given the essential role of *ucr-2.3* and mitochondria in the germline, we next asked if
335 simply general germline function was also essential for mediating cell nonautonomous UPR^{MT}
336 signaling. We tested this using genetic and pharmacological methods to deplete the germline in *C.*
337 *elegans*. For genetics, we generated germline deficient animals using two temperature sensitive
338 mutations *glp-4(bn2)* and *glp-1(e2141ts)*, which both restrict germ cell proliferation at the
339 restrictive temperature of 25 °C (Beanan and Strome, 1992; Mello et al., 1994). We then asked
340 whether germline deficient animals also have suppressed the cell nonautonomous UPR^{MT} signaling
341 **(Fig 5A)**. Indeed, we observed that germline deficient animals through the *glp-1* and *glp-4*
342 temperature sensitive mutations suppress cell nonautonomous UPR^{MT} signaling in the neuronal
343 PolyQ40 stress model **(Fig 5A*i-ii*)**. Interestingly, the *glp-1(e2141ts)* allele is long-lived while *glp-*
344 *4(bn2)* is not (Greer et al., 2010; TeKippe and Aballay, 2010), decoupling germline-mediated
345 suppression of UPR^{MT} signaling from longevity mechanisms. In addition, we find that the *glp-*
346 *4(bn2)* restrictive mutation also suppresses cell nonautonomous UPR^{MT} signaling for the neuron-
347 specific *cco-1* knockdown model **(Fig 5A*iii*)**. For a pharmacological method, we used the drug
348 FUDR to ablate the germline through prohibiting DNA replication, especially of mitochondria in
349 the developing germline (Tsang and Lemire, 2002) **(Fig 5B)**. We found that FUDR treatment
350 depleted the germline of mitochondria **(Supp Fig 5A)** as well as suppressed cell nonautonomous
351 activation the UPR^{MT} in both the neuronal PolyQ40 and *cco-1* RNAi hairpin models **(Fig 5B)**.
352 Together, these data demonstrate that an intact germline is essential for cell nonautonomous
353 UPR^{MT} signaling.

354 We also tested the specificity of the germline in regulating cell nonautonomous stress
355 response signaling, like for the UPR^{ER} or HSR. We find that FUDR treatment did not appreciably
356 inhibit UPR^{ER} cell nonautonomous signaling in the UPR^{ER}, although it did decrease the HSR
357 model **(Supp Fig 5B)**. We observed that the FUDR-treated HSR model animals were small and
358 sick, so the lack of HSR signal may result from additional drug interactions with FUDR treatment.
359 We also tested whether genetic germline depletion via the *glp-4(bn2)* temperature sensitive
360 mutation also impacted cell nonautonomous signaling in the UPR^{ER} or HSR models. While we
361 found the signaling models to be more variable at the 25 °C restrictive temperature, we did not see
362 appreciable reduction in cell nonautonomous signaling like for the UPR^{MT} **(Supp Fig 5C)**. Overall,
363 these results suggest that depletion of the germline tissue or germline mitochondria specifically
364 inhibits cell nonautonomous UPR^{MT} stress signaling between neurons and the intestine.
365

366 ***ucr-2.3* mediates cell nonautonomous UPR^{MT} downstream of established neuronal factors in**
367 **UPR^{MT} signaling**

368 Having identified the critical role of germline mitochondria and germline-acting *ucr-2.3* in
369 mediating UPR^{MT} signaling between neurons and the intestine, we next asked whether germline
370 *ucr-2.3* functioned downstream of previously identified neuronal mitokine signaling factors
371 (Berendzen et al., 2016; Merkwirth et al., 2016; Zhang et al., 2018). For instance, neuronal
372 overexpression of the WNT ligand *egl-20* and the histone demethylase *jmjd-1.2* can activate
373 intestinal UPR^{MT} even in the absence of neuronal mitochondrial stress **(Fig 6A)** (Merkwirth et al.,
374 2016; Zhang et al., 2018). We find that loss of *ucr-2.3* suppressed intestinal UPR^{MT} activation even
375 in the presence of neuronal over-expression of *egl-20* and *jmjd-1.2* **(Fig 6B-C)**. This brings further
376 evidence placing the role of *ucr-2.3* in the germline downstream of these neuronal factors to

377 mediate cell non-autonomous UPR^{MT} signaling. Additionally, we find that germline RNAi-specific
378 knockdown of UPR^{MT} regulators, such as *atfs-1*, *egl-20*, and *jmjd-1.2,* do not suppress cell non-
379 autonomous UPR^{MT} signaling **(Supp Fig 6)**, suggesting that the germline has an independent role
380 from these other neuronal factors for mediating cell nonautonomous UPR^{MT}.

381 One of the factors we also considered that could signal to the germline was serotonin, a
382 neurotransmitter that is released by dense core vesicles and mediates cell nonautonomous
383 activation of intestinal UPR^{MT} upon neuronal mitochondrial stress (Berendzen et al., 2016). We
384 directly tested whether *ucr-2.3* acted downstream of serotonin signaling by testing whether
385 exogenous serotonin addition could rescue cell nonautonomous UPR^{MT} signaling between neurons
386 and the intestine. While we found that exogenous addition of serotonin (5-HT) could increase
387 intestinal UPR^{MT} signaling in the wildtype animal, loss of function in *ucr-2.3* prevented serotonin-
388 mediated activation of intestinal UPR^{MT} **(Fig 6D)**. Therefore, germline *ucr-2.3* functions not only
389 downstream of *egl-20* and *jmjd-1.2*, but also downstream of serotonin signaling pathways to
390 mediate intestinal UPR^{MT} activation upon neuronal mitochondrial stress.

391

392 **Germline mitochondria regulate intestinal UPR^{MT} activation through altering lipid**
393 **metabolic and transport pathways**

394 Although our data indicate the *ucr-2.3* works downstream of the neuronal factors in
395 regulating intestinal UPR^{MT} activation, our data do not rule out the possibility that *ucr-2.3* works
396 in parallel with the neuronal factors to coordinate UPR^{MT} induction in peripheral cell types. In
397 this scenario, a signal might be sent from the germline to work with WNT signaling in peripheral
398 cells to specifically induce the UPR^{MT} and not developmental programs mediated by canonical
399 WNT signaling.

400 To identify what signals could be sent from the germline to regulate UPR^{MT} induction in
401 the intestine, we considered existing signaling models between the germline and the somatic
402 tissues, such as through lipid metabolism, steroid hormones, or piRNAs (Berman and Kenyon,
403 2006; Goudeau et al., 2011; Han et al., 2017; Lapierre et al., 2011; Shi and Murphy, 2023; Wang
404 et al., 2008). We were particularly motivated to explore a lipid-based germline signaling model
405 since one of our initial observations of the *ucr-2.3* mutant was that it had drastically higher levels
406 of intestinal fat **(Fig 7A, Supp Fig 7A)**. Since *ucr-2.3* mutant animals have compromised germline
407 mitochondrial and tissue integrity, this is in alignment with reports by others that germline
408 deficient animals also have higher intestinal fat levels **(Supp Fig 7B)** (O'Rourke et al., 2009). In
409 addition, from an RNA-seq analysis comparing *ucr-2.3(uth252); rgef-1p::Q40::YFP* mutant
410 animals to *rgef-1p::Q40::YFP* alone, we found that many up-regulated transcripts in the *ucr-*
411 *2.3(uth252)* mutant animals were highly enriched in GO terms for metabolic processes, especially
412 those involving fatty acids and lipids **(Fig 7B)**. Therefore, we tested whether compromised
413 germline mitochondrial integrity resulted in suppressed intestinal UPR^{MT} activation through
414 altering lipid metabolic pathways in the intestine. We conducted a targeted RNAi screen of fatty
415 acid and lipid metabolic genes corresponding to the up-regulated GO terms in the *ucr-2.3(uth252)*
416 mutant. Surprisingly, we found that knockdown of *fat-2*, a Δ12 desaturase enzyme that converts
417 oleic acid to linoelic acid in the first step of polyunsaturated fatty acid (PUFA) synthesis in *C.*
418 *elegans* (Watts and Browse, 2002; Zhou et al., 2011), rescued nonautonomous UPR^{MT} signaling
419 in the *ucr-2.3(uth252)* mutant **(Fig 7C)**.

420 We also considered pathways involving direct transfer of lipid molecules between the
421 germline and the intestine, such as the *vit* family of vitellogenins are lipoproteins which transport
422 phospholipids, cholesterol, and other nutrients from the intestine to the germline (Perez and Lehner,

423 2019) and are the evolutionary ancestor of human apolipoprotein B (APOB) (Babin et al., 1999).
424 We find that the *vit* family genes (*vit-1, 2, 3, 5, 6*) are also transcriptionally up-regulated in the
425 *ucr-2.3* mutant RNA-seq dataset (mean $\log_2$(FC) = 0.669, SD = 0.191). Additionally, we find that
426 RNAi knockdown of the *vit* family genes, which redistributes lipids and increases lysosomal
427 lipolysis in the intestine (Seah et al., 2016), rescued intestinal UPR^{MT} activation in the *ucr-2.3*
428 mutant **(Supp Fig 7C)**.

429 Overall, we find that *ucr-2.3* mutant animals have up-regulated intestinal lipid levels and
430 metabolic genes, and manipulating lipid synthesis and transport pathways in the intestine can
431 rescue non-autonomous UPR^{MT} activation in the *ucr-2.3* mutant. This suggests a mode of lipid-
432 based signaling between germline mitochondria and the intestine, whereby germline mitochondrial
433 quality may be communicated to the intestine through lipid synthesis and transport pathways which
434 subsequently regulates UPR^{MT} activation. Indeed, previous work had shown that mitochondrial
435 stress signaling can be also regulated by ceramide and cardiolipin lipids levels (Kim et al., 2016),
436 suggesting a general principle of mitochondrial stress regulation by lipids.

437 Collectively our data propose a model in which the germline, through germline
438 mitochondria, integrates mitokine stress signals from the nervous system to regulate UPR^{MT} in
439 peripheral tissues, such as the intestine **(Fig 7D)**. This highlights the role of the germline as a
440 signaling tissue that actively communicates with the soma regarding mitochondrial stress to
441 influence organismal stress and metabolic phenotypes. We believe the evolutionary basis for this
442 neuron and germline signaling circuit may be to conserve overall organismal resources in the
443 somatic tissues. The need to activate energy-intensive, protective stress responses should only be
444 executed in the presence of a functioning germline to preserve progeny production and
445 continuation of the immortal germline. Without a functional germline, there would be no need to

446 activate these energy-intensive stress responses, and the UPR^{MT} is shut off to direct resources
447 elsewhere. On a broader level, we believe this signaling circuit has implications for how germ cells
448 and germline mitochondrial quality may be influenced by and respond to stresses occurring in the
449 somatic environment, such as with aging, metabolic disease, or infection.
450

451 **Discussion**

452 In this study, we have identified the importance of the germline, and particularly of
453 germline mitochondria, in mediating cell nonautonomous communication of mitochondrial stress
454 from the nervous system to peripheral cells. Using a genome-wide mutagenesis screen, we
455 identified the mitochondrial gene *ucr-2.3* as a novel regulator of cell nonautonomous UPR^{MT}
456 signaling between neurons and the intestine in *C. elegans*. Surprisingly, we find that *ucr-2.3*
457 mediates cell nonautonomous UPR^{MT} signaling through its activity in the germline tissue. Loss of
458 *ucr-2.3* activity in the germline compromises germline mitochondrial health, germline integrity,
459 and suppresses neuronal-to-intestinal communication of mitochondrial stress signals. Furthermore,
460 we find that *ucr-2.3* works downstream and independently of other identified neuronal mediators
461 of cell nonautonomous UPR^{MT} signaling such as serotonin and *egl-20*/WNT mechanisms. We also
462 observe that *ucr-2.3* and germline tissue integrity is specific to UPR^{MT} cell nonautonomous
463 signaling and is not a primary mediator for other forms of cell nonautonomous communication,
464 such as the UPR^{ER} or cytosolic HSR. This suggests that there is a specific relationship between
465 germline mitochondrial integrity and inter-tissue mitochondrial stress signaling in the somatic
466 tissues. Finally, we find that *ucr-2.3* activity in the germline may communicate to the intestine
467 through alteration of lipid metabolism pathways to regulate UPR^{MT} activation. We propose that

468 this germline-to-intestine signal could also direct WNT signaling factors from their role in
469 developmental programs to regulating UPR^{MT} activation (Zhang et al., 2018).

470 Overall, our data highlight the role of the germline tissue in mediating cell nonautonomous
471 mitochondrial stress signaling and specifically a specialized role for germline mitochondria. Our
472 results provide additional context for understanding the communication between germline and
473 somatic tissues in regulating organismal health, especially regarding mitochondrial quality. While
474 often regarded as two separate entities, the soma and the germline must engage in constant
475 communication with each other to ensure overall organismal health (Conine and Rando, 2022).
476 This can come in the form of small RNAs, nutrients, and other growth or stress cues that allow the
477 germline to adapt to sources of environmental or somatic stress and, conversely, allow the somatic
478 tissues to respond to changes in germline integrity. Several examples of soma-to-germline
479 communication pathways have been described in *C. elegans* (Calculli et al., 2021; Curran et al.,
480 2009; Shi and Murphy, 2023). Our work here illustrates a germline mitochondrial-specific
481 communication pathway that involves reshuffling of lipid transport and metabolism pathways in
482 the intestine in response to mitokine stress signals from neurons.

483 Our findings suggest two models for how the germline could mediate neuronal-to-intestinal
484 UPR^{MT} signaling **(Fig 7D)**. In one model ("Parallel Signaling"), the germline acts as an ON/OFF
485 switch for intestinal UPR^{MT} activation. In this model, peripheral activation of the UPR^{MT} requires
486 signals from the nervous system (e.g., WNT and serotonin) *and* a signal from an intact, healthy
487 germline. In another model ("Direct Signaling"), the germline could act as an intermediary tissue,
488 wherein the germline receives signals secreted by neurons experiencing mitochondrial stress,
489 processes these signals – perhaps through mitochondrial *ucr-2.3* activity – then emits an additional

490 signal to the intestine to regulate UPR^{MT} activation. In both models, the germline may regulate
491 intestinal activation of UPR^{MT} signaling through lipid transport and synthesis pathways.

492 Based on our findings, we cannot disprove either the Parallel or Direct Signaling model,
493 nor have we shown direct evidence that germline mitochondria can receive signals from neurons.
494 However, regarding the possibility of a Direct Signaling model, we do observe that germline
495 mitochondrial signaling operates downstream of serotonin **(Fig 6D)**. In addition, it had been
496 previously shown that in the same neuronal polyQ40 model of mitochondrial stress in *C. elegans*,
497 neuronal mitochondrial stress elevated mtDNA levels in germline mitochondria, which could be
498 transgenerationally inherited (Q. Zhang et al., 2021). Furthermore, components of the WNT
499 signaling pathway, such as the beta-catenin *bar-1,* were also shown to directly regulate oocyte
500 mitochondria mass and mtDNA levels (Q. Zhang et al., 2021). Serotonin signaling has also been
501 shown to directly improve oocyte quality in *C. elegans* and *D. melanogaster* (Aprison et al., 2023),
502 suggesting that a Direct Signaling route between neurons and germ tissue through serotonin-based
503 signaling could exist.

504 The mechanism for how *ucr-2.3* activity in the germline controls cell nonautonomous
505 UPR^{MT} remains to be explored. One possibility is that loss of *ucr-2.3* function leads to
506 compromised mitochondrial function in the germ cells **(Fig 2C, Fig 4D, Supp Fig 5A)**, leading to
507 a general depletion of germ cell proliferation and resulting germline tissue loss. This is reflected
508 in the very small brood size of *ucr-2.3* mutant animals **(Fig 4C)**. In this scenario, the loss of
509 functional *ucr-2.3* compromises general germline integrity, leading to a loss of cell
510 nonautonomous signaling. Indeed, we believe the germline-specific expression of *ucr-2.3* is why
511 only mutations in *ucr-2.3* mutants were uncovered in our screen, as opposed to its more
512 ubiquitously expressed (and germline excluded) paralogs *ucr-2.1/2.2*.

513 Beyond its role in the electron transport chain, there could also be a specific activity related
514 to *ucr-2.3* in generating a signal either required for germline mitochondrial integrity or germline-
515 to-intestine UPR^{MT} signaling. One possibility we considered is the predicted role of *ucr-2.3* as a
516 protease, as its protein sequence is predicted to belong to the M16 metallopeptidase family, which
517 includes mitochondrial processing peptidases. Indeed, the mammalian ortholog of *ucr-2.3*,
518 UQCRC2, is also predicted to have MPP-like (mitochondrial peptide processing) protease activity
519 in combination with UQCRC1 to cleave off the N-terminal MTS of UQCRFS1 (the Rieske Fe-S
520 protein) in the final steps of complex III assembly (Deng et al., 2001, 1998; Fernandez-Vizarra
521 and Zeviani, 2018). Whether *C. elegans* UCR-2.3 could also have an MPP-like role in complex III
522 assembly in germline mitochondria or have an additional peptidase role to generate peptide-like
523 signals in the context of mitochondrial stress are interesting hypotheses that should be further
524 explored. While it is intriguing to speculate that *ucr-2.3* is specific for the germline signal,
525 additional germline restricted ETC genes, such as *nduf-2.2* were also required **(Fig 4G)**. Therefore,
526 it is also possible that *nduf-2.2* and *ucr-2.3* work together to generate a germline specific signal,
527 or more likely, general mitochondrial integrity within the germline is the predominant source of
528 the signal to the intestine. While each possibility cannot be excluded, it is intriguing to speculate
529 that evolution has opted to restrict expression of a few, key ETC genes within the germline to help
530 coordinate signals to the soma. Whether mitochondrial ETC isoforms with tissue-specific
531 expression also exist in humans should also be explored.

532 While several reports of germline deficient animals have increased stress resistance for the
533 cytosolic HSR or lifespan phenotypes (Hsin and Kenyon, 1999; Labbadia and Morimoto, 2015),
534 we find the opposite for mitochondrial stress responses; specifically, that germline deficiency shuts
535 down UPR^{MT} signaling. We believe this specificity in germ cell regulation of mitochondrial stress

536 signaling may result from a special requirement of mitochondrial quality in the germline. Because
537 of the high abundance of mitochondria in germ cells and their important role in germ cell
538 maturation (Van Blerkom, 2011; N. Zhang et al., 2021), the integrity of the germline and its
539 consequential communication with other tissues may have a heavy reliance on mitochondrial
540 quality. Indeed, oocytes in *C. elegans*, *Xenopus*, and humans employ specialized mechanisms to
541 maintain mitochondrial quality and ensure integrity of the reproductive tissues (Colnaghi et al.,
542 2021; Cota and Murphy, 2021; Rodríguez-Nuevo et al., 2022). For instance, germline
543 mitochondria demonstrate a higher protein import capacity compared to somatic mitochondria in
544 *C. elegans* (Xin et al., 2022). Our results also highlight the importance of mitochondrial quality in
545 germ tissue and suggest the possibility that integrity of germline may also regulate stress signaling
546 pathways between the germline and somatic tissues. It will be important to understand whether
547 these germline-somatic mitochondrial stress signaling pathways also are relevant for other forms
548 of somatic stress besides proteotoxic PolyQ40 aggregation, such as obesity or infection, and what
549 implications stresses occurring in the somatic tissues may have on germline mitochondrial quality,
550 fertility or reproductive tissue health, and lipid metabolism.

551 Finally, it is intriguing to consider our results in the context of the "Disposable Soma
552 Theory" which contends that there is an energetic trade-off between somatic maintenance and
553 reproductive health. By this theory, animals lacking a germline should be able to invest more
554 energetic resources to health maintenance in the somatic tissues, leading to increased longevity
555 and stress resistance. Our observations provide another layer of complexity to this theory by
556 contending that there may be an energetic triage occurring in response to loss of germline tissue.
557 While loss of germline tissue or *ucr-2.3* may lead to the up-regulation of certain stress responses,
558 it leads to an intestinal UPR^{MT} shutdown. This may operate through signaling mechanisms specific

559 to mitochondrial health or mitochondrial substrate requirements for metabolism no longer
560 necessary in an infertile organism. Thus, this intestinal UPR^{MT} shut off could be an adaptive
561 mechanism to conserve organismal resources but have additional consequences on fat metabolism
562 in somatic tissues. Whether infertility or compromised reproductive tissues health may have
563 similar consequences in mitochondrial or metabolic states in humans is of great future interest,
564 especially given existing connections between obesity and sterility/infertility in humans (Carrageta
565 et al., 2019; Ozcan Dag and Dilbaz, 2015; Whon et al., 2021).
566

567 **Acknowledgements:** We thank all members of the Dillin lab, Dr. Jeremy Chang, Dr. Veerle
568 Rottiers, and Dr. Malene Hansen for their feedback on the project. We acknowledge support by
569 the Howard Hughes Medical Institute (J.K.D., C.G.M., L.J., A.D.) and the National Institutes of
570 Health (A.D., B.M.W.). K.S. is supported by a K99/R00 Pathway to Independence Award
571 (K99AG071935). C.K.T. is supported by a NIH F32 Postdoctoral Fellowship (5F32AG069388-
572 03). H.Z. is supported by the Larry L. Hillblom Foundation Postdoctoral Fellowship (2020-A-018-
573 FEL) and the Glenn Foundation for Medical Research Postdoctoral Fellowship.
574

575 **Figure titles and legends**

576 **Figure 1: Mutagenesis screen reveals the requirement of *ucr-2.3* in neuron-to-intestine**
577 **UPR^{MT} signaling**

578 a. Schematic of cell nonautonomous UPR^{MT} signaling model in *C. elegans*. Through an inter-
579 tissue signaling mechanism, neuron-specific mitochondrial stress activates the UPR^{MT} in
580 the intestine of *C. elegans*. Neuronal mitochondrial stress can be induced by neuron-
581 specific expression of a mutant, aggregation-prone PolyQ40 protein (*rgef-1p::Q40::YFP*)

582 or neuron-specific knockdown mitochondrial genes like complex IV subunit *cco-1*. UPR^{MT}
583 activation can be detected by use of a transcriptional reporter *hsp-6p::GFP*. See text for
584 more details.

585 b. Fluorescence imaging and quantification of *rgef-1p::Q40::YFP; hsp-6p::GFP* animals
586 with and without loss of function mutation *ucr-2.3(uth252)*. The Q40::YFP signal in *C.*
587 *elegans* neurons is denoted with an orange arrowhead. The UPR^{MT} transcriptional reporter
588 signal (GFP expression driven by the *hsp-6* promoter) is denoted with the red brackets.
589 Significance determined by Welch's unpaired t-test, ****$p<0.0001$; $n > 3$.

590 c. Fluorescence imaging and quantification of *sid-1(qt9); rab-3p::cco-1* hairpin*; hsp-*
591 *6p::GFP* animals with and without loss of function mutation *ucr-2.3(uth252)*. Significance
592 determined by Welch's unpaired t-test, ****$p<0.0001$; $n > 3$.

593 d. Fluorescence imaging and quantification of *hsp-6p::GFP* animals with and without loss of
594 function mutation *ucr-2.3(uth252)* fed *cco-1* RNAi . Significance determined by Welch's
595 unpaired t-test, $p = 0.6372$; $n > 3$.

596

597 **Figure 2: UCR-2.3 is a mitochondrial protein in *C. elegans* with a novel role in cell**
598 **nonautonomous mitochondrial stress signaling**

599 a. *(i)* Schematic of sub-cellular fractionation of a *C. elegans* strain with a HA-tag inserted at
600 the C-terminus of the *ucr-2.3* genomic locus using CRISPR/Cas9 genomic editing.
601 Cytosolic and mitochondrial fractions were run on a western blot probed with an HA
602 antibody (to detect UCR-2.3 protein), a NDUFS3 antibody (to detect an established
603 mitochondrial ETC protein), and an α-tubulin antibody (to detect an established cytosolic
604 protein).

605 b. *(i)* Live-cell imaging showing sub-cellular localization of *C. elegans* UCR-2.3 in human
606 RPE1 hTert cells transduced with *C. elegans* UCR2.3 tagged with mNeonGreen (UCR-
607 2.3-mNG) and OMP25 tagged with BFP (OMP25-tagBFP2). Scale bar is 5 μm. *(ii)* Close
608 up of two example regions shown in *(i)*. Scale bar is 1 μm. Data shown is representative of
609 at least two independent imaging experiments with 5-10 images collected per cell line.
610 c. Measurement of mitochondrial respiration or OCR (oxygen consumption rate) between
611 wildtype and the *ucr-2.3(uth252)* mutant in the *rgef-1p::Q40::YFP; hsp-6p::GFP* genetic
612 background. Significance determined by Welch's unpaired t-test, ** $p = 0.0079$; $n > 4$.
613 d. Fluorescence imaging comparison of intestinal UPR^{MT} between wildtype and a *ucr-2.3*
614 mutant with the predicted mitochondrial targeting sequence (MTS) deleted *ucr-2.3(ΔMTS)*,
615 all in the *rgef-1p::Q40::YFP; hsp-6p::GFP* genetic background. Significance determined
616 by Welch's unpaired t-test, * $p = 0.0103$; $n = 3$.
617
618 **Figure 3: *ucr-2.3* is part of the UCR-2 family of gene paralogs that differ in their tissue**
619 **expression and role in cell nonautonomous UPR^{MT} signaling**
620 a. Human UQCRC2 is homologous to a family of UCR-2 genes in *C. elegans* including *ucr-*
621 *2.1*, *ucr-2.2*, and *ucr-2.3*.
622 b. *(i)* Fluorescence imaging of comparing the loss of function mutations in the UCR-2 family
623 on cell nonautonomous UPR^{MT} signaling. All mutations showed are nonsense-mediated
624 decay mutations generated via CRISPR/Cas9 editing. Quantification (*ii*). Significance
625 determined by Welch's unpaired t-test. *$p < 0.05$, ****$p < 0.0001$; $n = 3$.
626 c. Fluorescence imaging comparison of tissue expression patterns across the UCR-2 family
627 genes using an endogenous transcriptional reporter for each gene: *ucr-2.1* (*i*), *ucr-2.2* (*ii*),

628 and *ucr-2.3* (*iii*). To generate each transcriptional reporter, a mCherry::GSG linker::F2A
629 sequence was inserted between the gene promoter and coding region at the genomic locus
630 using CRISPR/Cas9 editing.
631 d. Close up head images of the endogenous transcriptional reporter as described in (C).
632 e. Close up head imaging of *ucr-2.3* endogenous transcriptional reporter crossed to a *rgef-*
633 *1p::GFP* reporter strain, expressing GFP in neurons.
634
635 **Figure 4: *ucr-2.3* acts in the germline to mediate cell nonautonomous UPR^{MT} signaling and**
636 **germline mitochondrial integrity**
637 a. Schematic of single-copy (mosSCI) tissue-specific rescue experiment. *ucr-2.3(ok3073)*
638 mutant was crossed to strains containing an integrated, single-copy (mosSCI) of wildtype
639 *ucr-2.3* driven by either a neuron-specific (*rgef-1p*) or germline-specific (*pie-1p*) promoter,
640 all in the *rgef-1p::Q40::YFP; hsp-6p::GFP* genetic background.
641 b. Fluorescence imaging comparison of tissue-specific mosSCI rescue experiment in the *rgef-*
642 *1p::Q40::YFP; hsp-6p::GFP* genetic background for the *ucr-2.3(ok3073)* mutation with
643 tissue-specific rescue of wild-type *ucr-2.3* expressed in either in neurons (+ *rgef-1p*) or the
644 germline (+ *pie-1p*) *(i)*. Significance determined by Welch's unpaired t-test, ****p< 0.0001.
645 All non-significant p values > 0.3924. Quantification *(ii)*. n = 3.
646 c. Measurement of total brood size among wildtype, *ucr-2.3(ok3073)* loss of function mutant,
647 and tissue-specific rescue with wild-type *ucr-2.3* expressed either in neurons (*rgef-1p::ucr-*
648 *2.3*) or the germline (*pie-1p::ucr-2.3*), all in the *rgef-1p::Q40::YFP; hsp-6p::GFP* genetic
649 background. Significance determined by Welch's unpaired t-test, **p=0.0011. All non-
650 significant p values > 0.1507. n = 3.

651 d. Measurement of mitochondrial respiration (oxygen consumption rate) for wildtype and the
652 *ucr-2.3(uth252)* mutant with and without an intact germline, all in the *rgef-1p::Q40::YFP;*
653 *hsp-6p::GFP* genetic background. The germline was genetically ablated via the *glp-4(bn2)*
654 temperature-sensitive mutant strain and conducting the entire experiment at the restrictive
655 temperature 25°C. All strains were fed control HT115 RNAi bacteria, except for the *glp-*
656 *4(bn2)* mutant animals fed *cco-1* RNAi. Significance determined by Welch's unpaired t-
657 test, **p = 0.0019, ****p < 0.0001, non-significant p = 0.1051. n = 3.
658 e. Fluorescence widefield imaging of *pie-1p::tomm-20::mKate2* germline mitochondrial
659 reporter strain with and without the *ucr-2.3(uth252)* mutation *(i)*. Scale bar = 25 μm. Distal
660 germ cells (green arrowhead) and oocytes (blue arrowhead) are shown in zoomed in images
661 *(ii)*. Scale bar = 10 μm. Images shown are representative of at least 5-10 animals imaged
662 per strain in at least three independent experiments each. Quantification of average
663 mitochondrial number *(iii)* and mitochondrial length *(iv)* between the wildtype and *ucr-*
664 *2.3(uth252)* mutant strain. Significance determined by Welch's unpaired t-test, **p =
665 0.0010, *p = 0.0205; n > 2.
666 f. Fluorescence imaging comparison of the *ucr-2.3(ok3073); rgef-1p::Q40::YFP; hsp-*
667 *6p::GFP* with and without the mosSCI rescue of germline-expressed wildtype *ucr-2.1*
668 (*pie-1p::ucr-2.1*). Significance determined by Welch's unpaired t-test, ***p=0.001; n =
669 2.
670 g. Fluorescence imaging comparison *(i)* and quantification *(ii)* of *rgef-1p::Q40::YFP;hsp-*
671 *6p::GFP* with and without the *nduf-2.2(uth312)* null mutation. *nduf-2.2* has enriched
672 expression to germline and neuronal tissues compared to its more ubiquitously expressed

673 counterpart *gas-1*. Significance determined by Welch's unpaired t-test, **p = 0.0015, n >
674 3.
675
676 **Figure 5: The germline, and especially germline mitochondria, is required for UPR^{MT} non-**
677 **autonomous signaling.**
678 a. Comparison of fluorescence imaging and quantification of intestinal UPR^{MT} signal in *(i)*
679 *glp-4(bn2)* or *(ii) glp-1(e2141)* temperature sensitive mutants, all in the *rgef-1p::Q40::YFP;*
680 *hsp-6p::GFP* background, or *(iii) glp-4(bn2)* in the *sid-1(qt9); rab-3p::cco-1 hairpin; hsp-*
681 *6p::GFP* background. Experiment conducted at the restrictive temperature 25 °C to deplete
682 the germline. Significance determined by Welch's unpaired t-test, ****, *** p<0.0001; n
683 = 3.
684 b. Comparison of fluorescence imaging and quantification of intestinal UPR^{MT} signal upon
685 FUDR treatment for germline mitochondria depletion in the *(i) rgef-1p::Q40::YFP; hsp-*
686 *6p::GFP* background or the *(ii) glp-4(bn2)* in the *sid-1(qt9); rab-3p::cco-1 hairpin; hsp-*
687 *6p::GFP* background. Significance determined by Welch's unpaired t-test, **p = 0.0034 ,
688 **** p<0.0001; n = 3.
689
690 **Figure 6: *ucr-2.3* operates downstream of established neuronal factors in mediating cell**
691 **nonautonomous UPR^{MT}**
692 a. Schematic of known neuronal molecular players that mediate cell nonautonomous UPR^{MT}
693 signaling between neurons and the intestine in *C. elegans.*

694 b. Fluorescence imaging comparison and quantification of intestinal UPR^{MT} signal in the
695 *rgef-1p::jmjd-1.2; hsp-6p::GFP* strain with and without the *ucr-2.3(uth252)* mutation.
696 Significance determined by Welch's unpaired t-test, ***p=0.0004; n = 3.
697 c. Fluorescence imaging comparison and quantification of intestinal UPR^{MT} signal in the
698 *rgef-1p::egl-20; hsp-6p::GFP* strain with and without the *ucr-2.3(uth252)* mutation
699 Significance determined by Welch's unpaired t-test, **p=0.0052; n = 3.
700 d. Fluorescence imaging comparison of intestinal UPR^{MT} signal for exogenous addition of
701 serotonin (5-HT) to *rgef-1p::Q40::YFP; hsp-6p::GFP* animals in the wildtype or *ucr-*
702 *2.3(uth252)* loss of function mutant. Quantification shows fold change in intestinal UPR^{MT}
703 fluorescence upon serotonin (5-HT) addition. Significance determined by Welch's
704 unpaired t-test, * p = 0.0296, non-significant p value = 0.3129. n = 4
705
706 **Figure 7: The germline regulates intestinal UPR^{MT} activation in the intestine through**
707 **alteration of lipid metabolic pathways.**
708 a. Comparison of lipid levels and quantification of Nile Red fluorescence between wildtype
709 and the *ucr-2.3(uth252)* mutant. Significance determined by Welch's unpaired t-test,
710 ****p <0.0001; n = 3.
711 b. Enriched GO terms (biological process) in up-regulated transcripts in the *ucr-2.3(uth252);*
712 *rgef-1p::Q40::YFP* mutant compared to *rgef-1p::Q40::YFP* alone. Shown are Fold
713 enrichment values determined by the PANTHER statistical overrepresentation test.
714 c. Fluorescence comparison of *ucr-2.3(uth252); rgef-1p::Q40::YFP; hsp-6p::GFP* animals
715 on control or *fat-2* RNAi. Significance determined by Welch's unpaired t-test, **p =
716 0.0020; n = 2.

717 d. Proposed model for how germline mitochondria mediate neuron-to-intestine UPR^{MT} stress
718 signaling. *(i)* Parallel Signaling pathway (Dashed lines): Neurons can communicate to the
719 intestine, or the germline. Simultaneously, the germline acts as a master switch to control
720 "ON"/"OFF" ability for the UPR^{MT} to be activated in the intestine, regardless of presence
721 of other signals. *(ii)* Direct Signaling pathway (Solid lines): Neurons directly communicate
722 to the germline, which processes signals possibly through mitochondrial activity, then
723 sends a signal to the intestine to regulate UPR^{MT} activation.
724
725 **Supplementary Figure 1: Additional genetic evidence supporting loss of function mutations**
726 **in *ucr-2.3* suppress cell nonautonomous UPR^{MT} signaling in *C. elegans***
727 a. Fluorescence imaging comparison of the wildtype UPR^{MT} cell nonautonomous reporter
728 strain *rgef-1p::Q40::YFP;hsp-6p::GFP* to the EMS mutant obtained in the suppressor
729 screen *uth16*. n> 3.
730 b. Fluorescence imaging comparison of a loss of function mutation in *ucr-2.3(uth214)*
731 generated by CRISPR/Cas9 genome editing to a non-edited, wildtype strain of *rgef-*
732 *1p::Q40::YFP;hsp-6p::GFP*. n > 3.
733 c. Fluorescence imaging comparison and quantification of a large deletion mutation in *ucr-*
734 *2.3* compared to a wildtype strain of *rgef-1p::Q40::YFP;hsp-6p::GFP*. Significance
735 determined by Welch's unpaired t-test, p = 0.0010; n > 3.
736 d. qPCR comparison of *ucr-2.3* expression levels in wildtype and *ucr-2.3(uth252)* mutant
737 animals in the *rgef-1p::Q40::YFP; hsp-6p::GFP* genetic background. Transcript levels
738 normalized by *rpl-32*. Significance determined by Welch's unpaired t-test, **p=0.0016.

739 e. Fluorescence imaging showing autonomous UPR^{MT} activation comparing wildtype and
740 *ucr-2.3(uth252)* animals fed *cco-1* RNAi in the *rgef-1p::Q40::YFP; hsp-6p::GFP* genetic
741 background. n > 3.
742 f. Schematic describing genetic changes in all shown mutant alleles of *ucr-2.3*.
743 g. Fluorescence comparison of intestinal UPR^{MT} signal in wildtype and *ucr-2.3(uth252)*
744 mutant animals over adult aging (Day 1 – 4 of adulthood). n > 3.
745
746 **Supplementary Figure 2: *ucr-2.3* loss of function does not suppress UPR^{ER} or cytosolic HSR**
747 **cell nonautonomous signaling**
748 a. Fluorescence imaging comparison of the cell nonautonomous UPR^{ER} reporter strain (*rgef-*
749 *1p::xbp-1s OE; hsp-4p::GFP*) with and without the *ucr-2.3(uth252)* loss of function
750 mutation. Significance determined by Welch's unpaired t-test, ** p = 0.0055; n = 3.
751 b. Fluorescence imaging comparison of the cell nonautonomous HSR reporter strain (*rab-*
752 *3p::hsf-1 OE; hsp-16p::GFP)* with and without the *ucr-2.3(uth252)* loss of function
753 mutation. Significance determined by Welch's unpaired t-test, **** p < 0.0001; n = 2.
754 c. Fluorescence imaging showing UPR^{MT} activation in the absence of mitochondrial stress
755 (basal condition). Shown are wildtype and *ucr-2.3(uth252)* animals fed control RNAi in
756 the *hsp-6p::GFP* UPR^{MT} reporter genetic background. Significance determined by
757 Welch's unpaired t-test, p = 0.6179; n = 3.
758 d. qPCR comparison of *ucr-2.3* expression levels in wildtype and *ucr-2.3(ΔMTS)* mutant
759 animals in the *rgef-1p::Q40::YFP; hsp-6p::GFP* genetic background. Transcript levels
760 normalized by *rpl-32*. Significance determined by Welch's unpaired t-test, p = 0.1603.
761

762 **Supplementary Figure 3: *ucr-2.1* and *ucr-2.2* are functionally redundant and display similar**
763 **tissue expression patterns but differ from *ucr-2.3***

764 a. Measurement of mitochondrial respiration (oxygen consumption rate) upon *ucr-2.1* and
765 *ucr-2.2* single and double RNAi knockdown in the *hsp-6p::GFP* genetic background.
766 Significance determined by Welch's unpaired t-test. ****p<0.0001, non-significant p
767 values > 0.4; n = 3.

768 b. Fluorescence imaging comparison of UPR^{MT} activation from *ucr-2.1* and *ucr-2.2* single
769 and double RNAi knockdowns in the *hsp-6p::GFP* UPR^{MT} reporter strain. n = 3.

770 c. Fluorescence imaging comparison of UPR^{MT} activation from *ucr-2.1* and *ucr-2.2* single
771 and double RNAi knockdowns in the *ucr-2.3(uth252); rgef-1p::Q40::YFP; hsp-6p::GFP*
772 genetic background. n = 3.

773 d. qPCR measurement of relative transcript levels of the *ucr-2* family genes between the *ucr-*
774 *2.3(uth252)* loss of function mutant and wildtype in the *rgef-1p::Q40::YFP; hsp-6p::GFP*
775 genetic background.

776 e. qPCR measurement of relative transcript levels of the *ucr-2* family genes between the *ucr-*
777 *2.1(uth267)* mutant *(i)* and *ucr-2.2(uth263)* mutant *(ii)* and wildtype with RNAi single and
778 double knockdown of *ucr-2.1* and *ucr-2.2 (iii)* in the *rgef-1p::Q40::YFP; hsp-6p::GFP*
779 genetic background.

780 f. Comparison of tissue-expression profiles for the UCR-2 family genes. Plots were generated
781 using the Worm tissue expression prediction web interface (Kaletsky et al., 2018) (http://
782 https://worm.princeton.edu/).

783

784 **Supplementary Figure 4: Additional genetic evidence supporting a germline-specific role for**
785 ***ucr-2.3* and germline mitochondria in mediating cell nonautonomous UPR^{MT}**

786 a. *(i)* Fluorescence imaging comparison of intestinal UPR^{MT} signal between *ucr-2.3* excised
787 only in neurons using FLP/FRT recombination (*ucr-2.3(FRT); rgef-1p::FLP*) compared to
788 *ucr-2.3* with the FRT sites alone *ucr-2.3(FRT)*, all in the *rgef-1p::Q40::YFP; hsp-6p::GFP*
789 genetic background. Wildtype and *ucr-2.3(uth252)* loss of function mutant displayed for
790 comparison. *(ii)* Quantification. Significance determined by Welch's unpaired t-test,
791 **p=0.0052, non-significant p values > 0.4. n = 3. *(iii)* DNA gel displaying excised *ucr-*
792 *2.3* upon FLP/FRT recombination by PCR genotyping the *ucr-2.3* genetic locus in each
793 strain listed.

794 b. Comparison of tissue-expression profiles for the *nduf-2* family genes (*gas-1/nduf-2.1*, *nduf-*
795 *2.2*). Plots were generated using the Worm tissue expression prediction web interface
796 (Kaletsky et al., 2018) (https://worm.princeton.edu/).

797 c. Fluorescence imaging showing autonomous UPR^{MT} activation comparing wildtype and
798 *nduf-2.2(uth312)* animals fed *cco-1* RNAi in the *rgef-1p::Q40::YFP;hsp-6p::GFP* genetic
799 background. n = 2.

800

801 **Supplementary Figure 5: Additional evidence supporting a specific role for the germline in**
802 **mediating UPR^{MT} signaling**

803 a. Fluorescence widefield imaging of *pie-1p::tomm-20::mKate2* germline mitochondrial
804 reporter strain with and without FUDR treatment.

805 b. Fluorescence imaging comparison and quantification of the cell nonautonomous UPR^{ER} *(i)*
806 and cytosolic HSR *(ii)* reporter strains upon germline depletion by FUDR treatment.

807 Significance determined by Welch's unpaired t-test, *(i)* p = 0.5250. *(ii)* **** p < 0.0001. n
808 = 3.
809 c. Fluorescence imaging comparison and quantification of the cell nonautonomous UPR^{ER}
810 and HSR reporter strains upon genetic germline depletion by the *glp-4(bn2)* temperature
811 sensitive mutation at the restrictive temperature 25 °C. Images shown are representative of
812 three independent experiments. Quantification displays average fluorescence values for
813 each strain from three independent experiments. Significance determined by Welch's
814 paired t-test across the three independent experiments, *(i)* p = 0.7477; *(ii)* p = 0.6100.
815
816 **Supplementary Figure 6: Germline-specific knockdown of known UPR^{MT} and mitokine**
817 **factors does not suppress nonautonomous UPR^{MT} signaling**
818 a. *(i)* Fluorescence imaging comparison of intestinal UPR^{MT} signal for RNAi knockdown of
819 UPR^{MT} factors *atfs-1*, *egl-20*, and *jmjd-1.2* in a germline-specific RNAi strain (Zou et al.,
820 2019) crossed to the cell nonautonomous UPR^{MT} reporter: *sun-1p::rde-1; rde-1(mkc36);*
821 *rgef-1p::Q40::YFP; hsp-6p::GFP*. *(ii)* RNAi knockdown of the same UPR^{MT} factors in the
822 standard cell nonautonomous UPR^{MT} reporter *rgef-1p::Q40::YFP; hsp-6p::GFP*. n = 3.
823
824 **Supplementary Figure 7: Increased intestinal fat levels in *ucr-2.3* loss of function and**
825 **germline deficient animals**
826 a. Oil Red O staining and quantification of lipid levels in wildtype or *ucr-2.3(uth252)* mutant
827 animals. Significance determined by Welch's unpaired t-test, ** p = 0.0185; n = 2.
828 b. Comparison of lipid levels and quantification of Nile Red fluorescence between wildtype
829 and germline deficient animals *glp-1(e2141)* and *glp-4(bn2)*. Experiment conducted at the

830 restrictive temperature 25 °C to deplete the germline. Significance determined by Welch's
831 unpaired t-test, ****p <0.0001; n = 2.
832 c. Fluorescence comparison of *ucr-2.3(uth252); rgef-1p::Q40::YFP; hsp-6p::GFP* animals
833 on control or *vit-1, vit-3, vit-5* RNAi. Significance determined by Welch's unpaired t-test,
834 **** p < 0.0001, *** p < 0.001; n > 3.
835

836 **Methods**

837 ***C. elegans* strain generation and maintenance**

838 *C. elegans* animals were fed standard OP50 bacteria and grown on standard NGM containing
839 media. For all RNAi knockdown experiments, *C. elegans* animals were fed HT115 bacteria
840 expressing dsRNA targeted to the gene of interest on NGM media containing IPTG and
841 appropriate antibiotics for selection of the dsRNA-containing plasmid. All strains were either
842 generated by this study, generated by SUNY Biotech, or ordered from the Caenorhabditis Genetics
843 Center (CGC). The only exception is the SJZ106 strain (*foxSi27[pie-*
844 *1p::tomm20::mKate2::HA::tbb-2 3'UTR]*), which was a kind gift from Dr. Steve Zuryn (The
845 University of Queensland). CRISPR-edited strains were either ordered from SUNY Biotech or
846 generated by this study following standard *C. elegans* CRISPR/Cas9 genome editing protocols
847 (Arribere et al., 2014) and the Alt-R CRISPR-Cas9 system (IDT). Briefly, Cas9 protein (UC
848 Berkeley QB3 MacroLab) was combined with Alt-R CRISPR tracrRNA, a crRNA mixture
849 (targeted to our gene of interest and *dpy-10*), and ssDNA repair template mixture (again, targeted
850 to our gene of interest and *dpy-10*) as a ribonucleoprotein complex and injected into the gonad of
851 L4 stage *C. elegans* hermaphrodites. This allowed us to select "jackpot" broods containing many
852 F1 animals with "roller" or "dumpy" phenotypes to improve efficiency in selection of broods with

853 edited genomes. mosSCI integration of strains were generated following standard procedures
854 (Frøkjær-Jensen et al., 2008). Briefly, constructs of interest were cloned into the pCFJ356 mosSCI
855 plasmid backbone. A DNA mixture of the mosSCI plasmid of interest, the pCFJ601 plasmid
856 (containing the mosSCI transposase), and mCherry expressing plasmids (to eliminate non-
857 integrated, array animals) was injected into the gonad of young, "uncoordinated" EG6703 animals.
858 Resulting progeny were screened for broods that yielded only "mover" animals with no mCherry-
859 expressing arrays.
860
861 **Animal synchronization and maintenance**
862 Unless stated, all experiments were performed with synchronization using a standard hypochlorite
863 treatment protocol. Briefly, animals were washed off NGM plates with a M9 solution and bleached
864 with 1.8% sodium hypochlorite solution until all animal carcasses were disintegrated. Resulting
865 eggs were washed five times with M9 solution using centrifugation and eggs were plated on
866 respective plates for the experiments. All experiments were conducted at 20 °C except for germline
867 ablation experiments with temperature sensitive mutants, which were done at the restrictive
868 temperature of 25 °C as indicated in figure legends.
869
870 **Mutagenesis screen**
871 *rgef-1p::Q40::YFP; hsp-6p::GFP* animals at the L4 stage were incubated with Ethyl-methyl
872 sulfonate (EMS, Sigma). Five plates of 250 F1 progeny each were selected to screen 2500 genomes.
873 F2 progeny were screened for suppression of *hsp-6p::GFP* signal in the intestine. Identified
874 suppressors were singled onto fresh plates and further screened for homozygous, recessive

875 mutations. Selected suppressor mutants were backcrossed to the parental strain carrying the
876 reporter and polyQ transgenes at least one time.
877
878 **Mutation mapping**
879 We followed a SNP-based whole genome sequencing method to identify putative causative
880 mutations in the suppressor mutants (Doitsidou et al., 2010). Briefly, we outcrossed suppressor
881 mutant strains with males from a Hawaiian CB4866 strain containing the *rgef-1p::Q40::YFP* and
882 *hsp-6p::GFP* transgenes. F2 progeny containing the suppression phenotype were selected and
883 allowed to self-fertilize for two generations. Then, genomic DNA was extracted from these
884 suppressor lines using the DNeasy kit (Qiagen) and sent to the Beijing Genomics Institute for WGS
885 on their Illumina HiSeq platform using single 90 nucleotide reads. Genomic data was analyzed
886 using MAQgene as previously described (Bigelow et al., 2009; Doitsidou et al., 2010).
887
888 **Fluorescence stereoscope imaging and quantification**
889 Animals were synchronized by hypochlorite treatment and hatched on either control or respective
890 HT115 RNAi bacteria. Animals were grown to Day 2 at 20 °C unless otherwise indicated, like for
891 the restrictive temperature experiments. For imaging experiments in the *rab-3p::hsf-1 OE; hsp-*
892 *16.2p::GFP* background, animals were heatshocked for imaging as had been previously published
893 (Gildea et al., 2022). Briefly, animals were hatched and allowed to develop at either 20 °C or 25
894 °C (if a temperature sensitive mutant). On the day of the experiment, animals were then
895 heatshocked at 34 °C for 2 hr, then let recover at their original temperature they developed at for
896 2 hr, then imaged. For imaging, D2 animals were anesthesized with 0.1 M sodium azide and lined
897 up on an NGM plate without a bacterial lawn. Animals were imaged using M250FA stereoscope

898 (Leica) under respective fluorescence. Animals were imaged at 250ms exposure under GFP
899 excitation fluorescence unless otherwise indicated. Quantification of intestinal GFP signal was
900 performed using ImageJ/FIJI by tracing the intestinal regions. Statistical analyses were performed
901 with GraphPad PRISM as described in the figure legends.
902

903 **Quantitative RT-PCR**

904 Synchronized animals were collected on Day 2 of adulthood and gravity washed in M9 buffer to
905 isolate adults and remove larvae. Animals were collected in three independent biological replicates
906 for one experiment. Washed animals were then frozen in TRIzol (Invitrogen) and freeze thawed
907 using liquid nitrogen. RNA was harvested from animals using a TRIzol-based extraction method
908 and RNA was purified using a RNeasy Mini Kit (Qiagen). cDNA was synthesized using the
909 QuantiTect Reverse Transcription Kit (Qiagen) using equivalent amounts of RNA per sample.
910 qPCR was performed using a standard curve protocol using SYBR Select Master Mix (Life
911 Technologies). Statistical analyses were performed with GraphPad PRISM as described in the
912 figure legends. Primers used are:

Gene	Forward primer	Reverse primer
rpl-32	AGGGAATTGATAACCGTGTCCGCA	TGTAGGACTGCATGAGGAGCATGT
ucr-2.1	TTGAACTAAACGGAGCCAC	TAAGTCCTTGCTTGTTGGC
ucr-2.2	CGAGGATGTGCTGCCAACTA	CGAAGTGCTGCTCTGCAAAT
ucr-2.3	GGAGTGTGGTGTCGTACCAG	GCGATAGTCTCCACCCCTGA

913

914 **Sub-cellular fractionation and western blotting**

915 Sub-cellular fractionation and mitochondrial enrichment of *C. elegans* lysates was performed as
916 previously described (Xin et al., 2022). Briefly, synchronized animals were mechanically
917 homogenized with a Dura-Grind Stainless Steel Dounce Trissue Grinder (Wheaton) in
918 mitochondrial extraction buffer (5 mM Tris-HCl / 7.4, 210 mM mannitol, 70 mM sucrose, and 0.1

919 mM EDTA) with protease inhibitor. Lysates were subject to differential centrifugation. Protein
920 concentration was measured using a Rapid Gold BCA kit (Pierce) before being loaded onto Tris-
921 Glycine 4-12% gels (Invitrogen). Gels were transferred using NuPAGE transfer buffer (Invitrogen)
922 onto nitrocellulose membranes (Biorad) and blocked with LI-COR Blocking Buffer (LI-COR)
923 with Tween. Membranes were probed with antibodies targeted to HA (Abcam, ab9110), NDUFS3
924 (Abcam, ab14711), and α Tubulin (Sigma, T9026).
925
926 **Cell culture, virus generation and transduction**
927 Human hTERT-RPE-1 PAC knockout cells (gifted by Andrew Holland (Lambrus et al., 2016))
928 were grown in DMEM:F-12 (Gibco) supplemented with 10% FBS (VWR Scientific), 1%
929 Glutamax (Gibco), 1% NEAA (Gibco), and 1% Penicillin/Streptomycin (Gibco). HEK-293T cells
930 were grown in DMEM (GIBCO) containing 10% FBS (VWR Scientific), 1% Glutamax (Gibco),
931 1% NEAA (Gibco), and 1% Penicillin/Streptomycin (Gibco). Cells were maintained at 37° C with
932 5% CO_2 at atmospheric O_2. Cultures were passaged enzymatically every 3-4 days using 0.25%
933 Trypsin (Gibco) diluted 1:3 in 1X PBS (Gibco). Trypsin was inactivated by cell media.
934
935 **Cloning of plasmids for cell culture**
936 *C. elegans* (human codon-optimized) UCR-2.3-mNeonGreen and OMP25-tagBFP2 were
937 synthesized as geneblocks (IDT), PCR amplified with Q5 polymerase (New England Biolabs) and
938 incubated with restriction enzyme-digested CD510-B1 plasmid (SystemBio) and assembled with
939 Gibson Assembly Master Mix (New England Biolabs).
940
941 **Generation and transduction of UCR-2.3 lentivirus**

942 Lentiviral plasmids encoding pCMV-OMP25-tagBFP2-EF1a-NEO and pUbC-UCR-2.3-
943 mNeonGreen-EF1a-Puro were transfected into HEK-293T cells with lentiviral packaging
944 plasmids with Lipofectamine 3000 (Invitrogen) according to standard lentiviral production
945 protocols. Viral supernatant was filtered through a 0.45 µm filter before transduction. RPE-1 cells
946 were transduced with lentivirus at an MOI of 0.3-0.5 (usually between 50-100 µL of virus/well)
947 and 10 µg/mL Polybrene (Sigma-Aldrich). After 48 hours, RPE-1 cell media was replaced and
948 grown in the presence of 1 µg/mL Puromycin (Gibco) or 100 µg/mL Geneticin (Gibco) for about
949 7 days and until all non-transduced control cells died.
950
951 **Live cell microscopy of human cells**
952 RPE-1 cells were seeded at 1.25 x 10^5 cells/dish onto Fibronectin-coated plates, 35-mm glass-
953 bottom dishes with #1.5 cover glass (Cellvis) 24 hours prior to imaging. Prior to live cell imaging,
954 cell medium was replaced with pre-warmed FluoroBrite DMEM (Gibco) supplemented with 10%
955 FBS, 1% Glutamax, 1% NEAA, 1% Penicillin/Streptomycin, 1 µM SYTO Deep Red Fluorescent
956 Nuclei Acid Stain (Invitrogen), and 1 µM Probenecid (Invitrogen). Imaging of live cells was
957 performed with a Zeiss Airyscan microscope LSM900 equipped with heated stage and
958 environmental chamber maintained at 37° C and 5% CO_2. Images were acquired using the
959 ZenBlue3.1 software followed by deconvolution and Airyscan processing, and further processed
960 using ImageJ/FIJI. Mander's colocalization coefficients are calculated using the Colocalization
961 threshold plug-in in ImageJ, in which the thresholds were set by the Costes Auto threshold method.
962
963 **Mitochondrial oxygen consumption assays**

964 All mitochondrial oxygen consumption rate assays (OCR) were performed using a Seahorse
965 XFe96 Analyzer (Agilent) at 20 °C following a previously published protocol . Briefly, the sensor
966 cartridge was calibrated the day before at room temperature, and appropriate drugs (NaN_3, FCCP)
967 were loaded into the injection ports. Day 2 adult animals were gravity washed with M9 buffer,
968 then loaded 10-20 animals per well into the cell culture plate. After respirometry run was
969 completed, the number of animals were counted per well to normalize the data. Statistical analyses
970 were performed with GraphPad PRISM as described in the figure legends.
971
972 **Fluorescence widefield microscopy of *C. elegans***
973 Slides for imaging were prepared by making a fresh flattened 5% agarose pad. Animals were
974 immobilized in 12 µl of 0.1% NaN_3, then sealed beneath a 22x22mm coverglass. 6-10 animals
975 were imaged per condition per experiment. Imaging was done using a Leica DM6 Thunder Imager
976 and processed using LAS X software automated Thunder small volume computational clearing.
977
978 **Brood size assay**
979 For each strain tested, five L4 animals were singled onto OP50 bacterial plates and kept at 20 °C
980 to lay. Animals were moved each day to new OP50 plates until Day 5. Progeny laid by each singled
981 animal were counted at the L4 or Day 1 life stage. Statistical analyses were performed with
982 GraphPad PRISM as described in the figure legends.
983
984 **Quantification of mitochondrial features using FIJI**
985 To quantify mitochondrial number and size in images of mitochondrial reporter worms, Z-stack
986 images were first projected into a single layer using the "Average Intensity" function. The "Auto

987 Local Threshold" function was applied with parameters of "method=Bernsen radius=15
988 parameter_1=0 parameter_2=0 white" to define mitochondria. The "Skeletonize (2D/3D)"
989 function was applied to extract individual mitochondrion and the "Analyze Skeleton (2D/3D)"
990 function was applied to count the number of these mitochondrial skeletons. To calculate
991 mitochondrial density, the area of the whole germline region was manually selected and measured
992 using FIJI (1 pixel area=0.010645 μm^2).
993
994 **Exogenous serotonin addition**
995 Exogenous serotonin addition was performed following a published procedure (Berendzen et al.,
996 2016). Serotonin hydrochloride (Sigma) was solubilized in MilliQ water and plated onto NGM
997 agar plates already containing control HT115 RNAi bacteria. Solubilized serotonin concentrations
998 were calculated so that the final serotonin concentration as stated considers the total agar volume
999 of the plate (approximately 9.9 ml). Seeded serotonin plates were allowed to dry overnight in the
1000 dark and plated with eggs harvested from a hypochlorite treatment for the experiment.
1001
1002 **5-Fluoro-2'deoxyuridine (FUDR) treatment**
1003 Eggs were harvested from hypochlorite treatment of animals and plated on control HT115 bacterial
1004 plates. 100 μL of 10 mg/mL FUDR was seeded onto the control HT115 bacterial lawn and let dry
1005 overnight at room temperature. At the L4 developmental stage, animals were moved onto the
1006 FUDR-treatment plates and let grown to Day 2 of adulthood for their respective experiment.
1007
1008 **Oil Red O and Nile Red staining**

1009 Lipid staining using Oil Red O or Nile Red was conducted following previously published protocol
1010 (Escorcia et al., 2018). Briefly, synchronized animals were grown to Day 2 on respective HT115
1011 RNAi media. Animals were washed in PBS-T, fixed in 40% isopropanol, then incubated with Oil
1012 Red O or Nile Red stain for 2 hours at room temperature shielded from light. Excess dye was
1013 washed off and animals were imaged via fluorescence stereoscope imaging for Nile Red using a
1014 M250FA stereoscope (Leica) or brightfield/colorimetric imaging for Oil Red O using a Revolve
1015 microscope (Echo). Quantification of signal was performed in ImageJ by tracing intestinal regions
1016 for fluorescent Nile Red images or Oil Red O colorimetric images. For quantification, Oil Red O
1017 images were transformed into the HIS color space using the Color Transformer 2 plugin and
1018 quantified in the (S) channel. Statistical analyses were performed with GraphPad PRISM as
1019 described in the figure legends.
1020

1021 **RNA-seq library preparation and analysis**

1022 RNA was prepared using methods similar to those for RT-qPCR as described above. RNASeq
1023 library preparation was performed using Roche products, KAPA Biosystems mRNA HyperPrep
1024 Kit and KAPA Unique Dual Index Adapters. Thermo Fisher Scientific NanoDrop and Qubit
1025 instruments were used to measure nucleic acid concentrations. Agilent BioAnalyzer was used to
1026 determine initial Total RNA and RNASeq library Quality. Single direction sequencing was
1027 performed using an Illumina NovaSeq, mode SP, SR100 at the Vincent J. Coates Genomic
1028 Sequencing Core at University of California, Berkeley. RNASeq analysis was performed by
1029 uploading .fastq files to the Galaxy web platform (The Galaxy Community et al., 2022), using the
1030 public server at usegalaxy.org and the *C. elegans* FASTA reference transcriptome
1031 Caenorhabditis_elegans.WBcel235.cdna.all.fa, downloaded from ensembl. Tools included

1032 Kallisto Quant v0.48.0+galaxy1 and DESeq2, v2.11.40.8+galaxy0(Afgan et al., 2018). GO term
1033 enrichment analysis was conducted using the PANTHER Overrepresentation Test on
1034 geneontology.org using genes significantly up-regulated with $\log_2(FC) > 1$. Only results with FDR
1035 p value < 0.05 were considered.
1036

1037 **References**
1038

1039 Afgan, E., Baker, D., Batut, B., van den Beek, M., Bouvier, D., Čech, M., Chilton, J., Clements,
1040 D., Coraor, N., Grüning, B.A., Guerler, A., Hillman-Jackson, J., Hiltemann, S., Jalili, V.,
1041 Rasche, H., Soranzo, N., Goecks, J., Taylor, J., Nekrutenko, A., Blankenberg, D., 2018.
1042 The Galaxy platform for accessible, reproducible and collaborative biomedical analyses:
1043 2018 update. Nucleic Acids Res. 46, W537–W544. https://doi.org/10.1093/nar/gky379

1044 Ahier, A., Dai, C.-Y., Tweedie, A., Bezawork-Geleta, A., Kirmes, I., Zuryn, S., 2018. Affinity
1045 purification of cell-specific mitochondria from whole animals resolves patterns of genetic
1046 mosaicism. Nat. Cell Biol. 20, 352–360. https://doi.org/10.1038/s41556-017-0023-x

1047 Aprison, E.Z., Dzitoyeva, S., Ruvinsky, I., 2023. Serotonergic signaling plays a deeply
1048 conserved role in improving oocyte quality. Dev. Biol. 499, 24–30.
1049 https://doi.org/10.1016/j.ydbio.2023.04.008

1050 Arribere, J.A., Bell, R.T., Fu, B.X.H., Artiles, K.L., Hartman, P.S., Fire, A.Z., 2014. Efficient
1051 Marker-Free Recovery of Custom Genetic Modifications with CRISPR/Cas9 in
1052 *Caenorhabditis elegans*. Genetics 198, 837–846.
1053 https://doi.org/10.1534/genetics.114.169730

1054 Babin, P.J., Bogerd, J., Kooiman, F.P., Van Marrewijk, W.J.A., Van Der Horst, D.J., 1999.
1055 Apolipophorin II/I, Apolipoprotein B, Vitellogenin, and Microsomal Triglyceride
1056 Transfer Protein Genes Are Derived from a Common Ancestor. J. Mol. Evol. 49, 150–
1057 160. https://doi.org/10.1007/PL00006528

1058 Beanan, M.J., Strome, S., 1992. Characterization of a germ-line proliferation mutation in *C.*
1059 *elegans*. Development 116, 755–766. https://doi.org/10.1242/dev.116.3.755

1060 Berendzen, K.M., Durieux, J., Shao, L.-W., Tian, Y., Kim, H., Wolff, S., Liu, Y., Dillin, A.,
1061 2016. Neuroendocrine Coordination of Mitochondrial Stress Signaling and Proteostasis.
1062 Cell 166, 1553-1563.e10. https://doi.org/10.1016/j.cell.2016.08.042

1063 Berman, J.R., Kenyon, C., 2006. Germ-Cell Loss Extends C. elegans Life Span through
1064 Regulation of DAF-16 by kri-1 and Lipophilic-Hormone Signaling. Cell 124, 1055–1068.
1065 https://doi.org/10.1016/j.cell.2006.01.039

1066 Bieri, G., Schroer, A.B., Villeda, S.A., 2023. Blood-to-brain communication in aging and
1067 rejuvenation. Nat. Neurosci. https://doi.org/10.1038/s41593-022-01238-8

1068 Bigelow, H., Doitsidou, M., Sarin, S., Hobert, O., 2009. MAQGene: software to facilitate C.
1069 elegans mutant genome sequence analysis. Nat. Methods 6, 549–549.
1070 https://doi.org/10.1038/nmeth.f.260

1071 Birch, J., Gil, J., 2020. Senescence and the SASP: many therapeutic avenues. Genes Dev. 34,
1072 1565–1576. https://doi.org/10.1101/gad.343129.120

1073 Calculli, G., Lee, H.J., Shen, K., Pham, U., Herholz, M., Trifunovic, A., Dillin, A., Vilchez, D.,
1074 2021. Systemic regulation of mitochondria by germline proteostasis prevents protein
1075 aggregation in the soma of *C. elegans*. Sci. Adv. 7, eabg3012.
1076 https://doi.org/10.1126/sciadv.abg3012

1077 Cao, J., Packer, J.S., Ramani, V., Cusanovich, D.A., Huynh, C., Daza, R., Qiu, X., Lee, C.,
1078 Furlan, S.N., Steemers, F.J., Adey, A., Waterston, R.H., Trapnell, C., Shendure, J., 2017.
1079 Comprehensive single-cell transcriptional profiling of a multicellular organism. Science
1080 357, 661–667. https://doi.org/10.1126/science.aam8940

1081 Carrageta, D.F., Oliveira, P.F., Alves, M.G., Monteiro, M.P., 2019. Obesity and male
1082 hypogonadism: Tales of a vicious cycle. Obes. Rev. 20, 1148–1158.
1083 https://doi.org/10.1111/obr.12863

1084 Castillo-Armengol, J., Fajas, L., Lopez-Mejia, I.C., 2019. Inter-organ communication: a
1085 gatekeeper for metabolic health. EMBO Rep. 20, e47903.
1086 https://doi.org/10.15252/embr.201947903

1087 Chandel, N.S., 2014. Mitochondria as signaling organelles. BMC Biol. 12, 34.
1088 https://doi.org/10.1186/1741-7007-12-34

1089 Colnaghi, M., Pomiankowski, A., Lane, N., 2021. The need for high-quality oocyte mitochondria
1090 at extreme ploidy dictates mammalian germline development. eLife 10, e69344.
1091 https://doi.org/10.7554/eLife.69344

1092 Conine, C.C., Rando, O.J., 2022. Soma-to-germline RNA communication. Nat. Rev. Genet. 23,
1093 73–88. https://doi.org/10.1038/s41576-021-00412-1

1094 Cota, V., Murphy, C.T., 2021. Fission and PINK-1-mediated mitophagy are required for
1095 Insulin/IGF-1 signaling mutant reproductive longevity (preprint). Genetics.
1096 https://doi.org/10.1101/2021.08.16.456566

1097 Curran, S.P., Wu, X., Riedel, C.G., Ruvkun, G., 2009. A soma-to-germline transformation in
1098 long-lived Caenorhabditis elegans mutants. Nature 459, 1079–1084.
1099 https://doi.org/10.1038/nature08106

1100 Deng, K., Shenoy, S.K., Tso, S.-C., Yu, L., Yu, C.-A., 2001. Reconstitution of Mitochondrial
1101 Processing Peptidase from the Core Proteins (Subunits I and II) of Bovine Heart
1102 Mitochondrial Cytochrome bc1 Complex. J. Biol. Chem. 276, 6499–6505.
1103 https://doi.org/10.1074/jbc.M007128200

1104 Deng, K., Zhang, L., Kachurin, A.M., Yu, L., Xia, D., Kim, H., Deisenhofer, J., Yu, C.-A., 1998.
1105 Activation of a Matrix Processing Peptidase from the Crystalline Cytochrome bc1
1106 Complex of Bovine Heart Mitochondria. J. Biol. Chem. 273, 20752–20757.
1107 https://doi.org/10.1074/jbc.273.33.20752

1108 Doitsidou, M., Poole, R.J., Sarin, S., Bigelow, H., Hobert, O., 2010. C. elegans Mutant
1109 Identification with a One-Step Whole-Genome-Sequencing and SNP Mapping Strategy.
1110 PLoS ONE 5, e15435. https://doi.org/10.1371/journal.pone.0015435

1111 Durieux, J., Wolff, S., Dillin, A., 2011. The Cell-Non-Autonomous Nature of Electron Transport
1112 Chain-Mediated Longevity. Cell 144, 79–91. https://doi.org/10.1016/j.cell.2010.12.016

1113 Escorcia, W., Ruter, D.L., Nhan, J., Curran, S.P., 2018. Quantification of Lipid Abundance and
1114 Evaluation of Lipid Distribution in Caenorhabditis elegans by Nile Red and Oil Red O
1115 Staining. J. Vis. Exp. 57352. https://doi.org/10.3791/57352

1116 Fernandez-Vizarra, E., Zeviani, M., 2018. Mitochondrial complex III Rieske Fe-S protein
1117 processing and assembly. Cell Cycle 17, 681–687.
1118 https://doi.org/10.1080/15384101.2017.1417707

1119 Frøkjær-Jensen, C., Wayne Davis, M., Hopkins, C.E., Newman, B.J., Thummel, J.M., Olesen,
1120 S.-P., Grunnet, M., Jorgensen, E.M., 2008. Single-copy insertion of transgenes in
1121 Caenorhabditis elegans. Nat. Genet. 40, 1375–1383. https://doi.org/10.1038/ng.248

1122 Fukasawa, Y., Tsuji, J., Fu, S.-C., Tomii, K., Horton, P., Imai, K., 2015. MitoFates: Improved
1123 Prediction of Mitochondrial Targeting Sequences and Their Cleavage Sites*. Mol. Cell.
1124 Proteomics 14, 1113–1126. https://doi.org/10.1074/mcp.M114.043083

1125 Gildea, H.K., Frankino, P.A., Tronnes, S.U., Pender, C.L., Durieux, J., Dishart, J.G., Choi, H.O.,
1126 Hunter, T.D., Cheung, S.S., Frakes, A.E., Sukarto, E., Wickham, K., Dillin, A., 2022.
1127 Glia of *C. elegans* coordinate a protective organismal heat shock response independent of
1128 the neuronal thermosensory circuit. Sci. Adv. 8, eabq3970.
1129 https://doi.org/10.1126/sciadv.abq3970

1130 Goudeau, J., Bellemin, S., Toselli-Mollereau, E., Shamalnasab, M., Chen, Y., Aguilaniu, H.,
1131 2011. Fatty Acid Desaturation Links Germ Cell Loss to Longevity Through NHR-
1132 80/HNF4 in C. elegans. PLoS Biol. 9, e1000599.
1133 https://doi.org/10.1371/journal.pbio.1000599

1134 Greer, E.L., Maures, T.J., Hauswirth, A.G., Green, E.M., Leeman, D.S., Maro, G.S., Han, S.,
1135 Banko, M.R., Gozani, O., Brunet, A., 2010. Members of the H3K4 trimethylation
1136 complex regulate lifespan in a germline-dependent manner in C. elegans. Nature 466,
1137 383–387. https://doi.org/10.1038/nature09195

1138 Han, S., Schroeder, E.A., Silva-García, C.G., Hebestreit, K., Mair, W.B., Brunet, A., 2017.
1139 Mono-unsaturated fatty acids link H3K4me3 modifiers to C. elegans lifespan. Nature
1140 544, 185–190. https://doi.org/10.1038/nature21686

1141 Horowitz, A.M., Fan, X., Bieri, G., Smith, L.K., Sanchez-Diaz, C.I., Schroer, A.B., Gontier, G.,
1142 Casaletto, K.B., Kramer, J.H., Williams, K.E., Villeda, S.A., 2020. Blood factors transfer
1143 beneficial effects of exercise on neurogenesis and cognition to the aged brain. Science
1144 369, 167–173. https://doi.org/10.1126/science.aaw2622

1145 Houtkooper, R.H., Mouchiroud, L., Ryu, D., Moullan, N., Katsyuba, E., Knott, G., Williams,
1146 R.W., Auwerx, J., 2013. Mitonuclear protein imbalance as a conserved longevity
1147 mechanism. Nature 497, 451–457. https://doi.org/10.1038/nature12188

1148 Howe, K.L., Bolt, B.J., Cain, S., Chan, J., Chen, W.J., Davis, P., Done, J., Down, T., Gao, S.,
1149 Grove, C., Harris, T.W., Kishore, R., Lee, R., Lomax, J., Li, Y., Muller, H.-M.,
1150 Nakamura, C., Nuin, P., Paulini, M., Raciti, D., Schindelman, G., Stanley, E., Tuli, M.A.,
1151 Van Auken, K., Wang, D., Wang, X., Williams, G., Wright, A., Yook, K., Berriman, M.,
1152 Kersey, P., Schedl, T., Stein, L., Sternberg, P.W., 2016. WormBase 2016: expanding to
1153 enable helminth genomic research. Nucleic Acids Res. 44, D774–D780.
1154 https://doi.org/10.1093/nar/gkv1217

1155 Hsin, H., Kenyon, C., 1999. Signals from the reproductive system regulate the lifespan of C.
1156 elegans. Nature 399, 362–366. https://doi.org/10.1038/20694

1157 Iwata, S., Lee, J.W., Okada, K., Lee, J.K., Iwata, M., Rasmussen, B., Link, T.A., Ramaswamy,
1158 S., Jap, B.K., 1998. Complete Structure of the 11-Subunit Bovine Mitochondrial
1159 Cytochrome bc_1 Complex. Science 281, 64–71.
1160 https://doi.org/10.1126/science.281.5373.64

1161 Jia, Q., Sieburth, D., 2021. Mitochondrial hydrogen peroxide positively regulates neuropeptide
1162 secretion during diet-induced activation of the oxidative stress response. Nat. Commun.
1163 12, 2304. https://doi.org/10.1038/s41467-021-22561-x

1164 Kaletsky, R., Yao, V., Williams, A., Runnels, A.M., Tadych, A., Zhou, S., Troyanskaya, O.G.,
1165 Murphy, C.T., 2018. Transcriptome analysis of adult Caenorhabditis elegans cells reveals
1166 tissue-specific gene and isoform expression. PLOS Genet. 14, e1007559.
1167 https://doi.org/10.1371/journal.pgen.1007559

1168 Kang, G.M., Min, S.H., Lee, C.H., Kim, J.Y., Lim, H.S., Choi, M.J., Jung, S.-B., Park, J.W.,
1169 Kim, S., Park, C.B., Dugu, H., Choi, J.H., Jang, W.H., Park, S.E., Cho, Y.M., Kim, J.G.,
1170 Kim, K.-G., Choi, C.S., Kim, Y.-B., Lee, C., Shong, M., Kim, M.-S., 2021. Mitohormesis
1171 in Hypothalamic POMC Neurons Mediates Regular Exercise-Induced High-Turnover
1172 Metabolism. Cell Metab. 33, 334-349.e6. https://doi.org/10.1016/j.cmet.2021.01.003

1173 Katsimpardi, L., Litterman, N.K., Schein, P.A., Miller, C.M., Loffredo, F.S., Wojtkiewicz, G.R.,
1174 Chen, J.W., Lee, R.T., Wagers, A.J., Rubin, L.L., 2014. Vascular and Neurogenic
1175 Rejuvenation of the Aging Mouse Brain by Young Systemic Factors. Science 344, 630–
1176 634. https://doi.org/10.1126/science.1251141

1177 Kim, H.-E., Grant, A.R., Simic, M.S., Kohnz, R.A., Nomura, D.K., Durieux, J., Riera, C.E.,
1178 Sanchez, M., Kapernick, E., Wolff, S., Dillin, A., 2016. Lipid Biosynthesis Coordinates a
1179 Mitochondrial-to-Cytosolic Stress Response. Cell 166, 1539-1552.e16.
1180 https://doi.org/10.1016/j.cell.2016.08.027

1181 Labbadia, J., Morimoto, R.I., 2015. Repression of the Heat Shock Response Is a Programmed
1182 Event at the Onset of Reproduction. Mol. Cell 59, 639–650.
1183 https://doi.org/10.1016/j.molcel.2015.06.027

1184 Lambrus, B.G., Daggubati, V., Uetake, Y., Scott, P.M., Clutario, K.M., Sluder, G., Holland, A.J.,
1185 2016. A USP28–53BP1–p53–p21 signaling axis arrests growth after centrosome loss or
1186 prolonged mitosis. J. Cell Biol. 214, 143–153. https://doi.org/10.1083/jcb.201604054

1187 Lapierre, L.R., Gelino, S., Meléndez, A., Hansen, M., 2011. Autophagy and Lipid Metabolism
1188 Coordinately Modulate Life Span in Germline-less C. elegans. Curr. Biol. 21, 1507–
1189 1514. https://doi.org/10.1016/j.cub.2011.07.042

1190 Macías-León, J., Askjaer, P., 2018. Efficient FLP-mediated germ-line recombination in C.
1191 elegans. Micropublication.

1192 Mello, C.C., Draper, B.W., Prless, J.R., 1994. The maternal genes apx-1 and glp-1 and
1193 establishment of dorsal-ventral polarity in the early C. elegans embryo. Cell 77, 95–106.
1194 https://doi.org/10.1016/0092-8674(94)90238-0

1195 Merkwirth, C., Jovaisaite, V., Durieux, J., Matilainen, O., Jordan, S.D., Quiros, P.M., Steffen,
1196 K.K., Williams, E.G., Mouchiroud, L., Tronnes, S.U., Murillo, V., Wolff, S.C., Shaw,
1197 R.J., Auwerx, J., Dillin, A., 2016. Two Conserved Histone Demethylases Regulate
1198 Mitochondrial Stress-Induced Longevity. Cell 165, 1209–1223.
1199 https://doi.org/10.1016/j.cell.2016.04.012

1200 Moehle, E.A., Shen, K., Dillin, A., 2019. Mitochondrial proteostasis in the context of cellular
1201 and organismal health and aging. J. Biol. Chem. 294, 5396–5407.
1202 https://doi.org/10.1074/jbc.TM117.000893

1203 Mottis, A., Herzig, S., Auwerx, J., 2019. Mitocellular communication: Shaping health and
1204 disease. Science 366, 827–832. https://doi.org/10.1126/science.aax3768

1205 Muñoz-Jiménez, C., Ayuso, C., Dobrzynska, A., Torres-Mendéz, A., Ruiz, P. de la C., Askjaer,
1206 P., 2017. An Efficient FLP-Based Toolkit for Spatiotemporal Control of Gene Expression
1207 in *Caenorhabditis elegans*. Genetics 206, 1763–1778.
1208 https://doi.org/10.1534/genetics.117.201012

1209 Nargund, A.M., Pellegrino, M.W., Fiorese, C.J., Baker, B.M., Haynes, C.M., 2012.
1210 Mitochondrial Import Efficiency of ATFS-1 Regulates Mitochondrial UPR Activation.
1211 Science 337, 587–590. https://doi.org/10.1126/science.1223560

1212 Nomura, H., Athauda, S.B.P., Wada, H., Maruyama, Y., Takahashi, K., Inoue, H., 2006.
1213 Identification and Reverse Genetic Analysis of Mitochondrial Processing Peptidase and
1214 the Core Protein of the Cytochrome bc1 Complex of Caenorhabditis elegans, a Model
1215 Parasitic Nematode. J. Biochem. (Tokyo) 139, 967–979.
1216 https://doi.org/10.1093/jb/mvj114

1217 O'Rourke, E.J., Soukas, A.A., Carr, C.E., Ruvkun, G., 2009. C. elegans Major Fats Are Stored in
1218 Vesicles Distinct from Lysosome-Related Organelles. Cell Metab. 10, 430–435.
1219 https://doi.org/10.1016/j.cmet.2009.10.002

1220 Owusu-Ansah, E., Song, W., Perrimon, N., 2013. Muscle Mitohormesis Promotes Longevity via
1221 Systemic Repression of Insulin Signaling. Cell 155, 699–712.
1222 https://doi.org/10.1016/j.cell.2013.09.021

1223 Ozcan Dag, Z., Dilbaz, B., 2015. Impact of obesity on infertility in women. J. Turk. Ger.
1224 Gynecol. Assoc. 16, 111–117. https://doi.org/10.5152/jtgga.2015.15232

1225 Ozek, C., Krolewski, R.C., Buchanan, S.M., Rubin, L.L., 2018. Growth Differentiation Factor 11
1226 treatment leads to neuronal and vascular improvements in the hippocampus of aged mice.
1227 Sci. Rep. 8, 17293. https://doi.org/10.1038/s41598-018-35716-6

1228 Perez, M.F., Lehner, B., 2019. Vitellogenins - Yolk Gene Function and Regulation in
1229 Caenorhabditis elegans. Front. Physiol. 10, 1067.
1230 https://doi.org/10.3389/fphys.2019.01067

1231 Rao, S., Schieber, A.M.P., O'Connor, C.P., Leblanc, M., Michel, D., Ayres, J.S., 2017.
1232 Pathogen-Mediated Inhibition of Anorexia Promotes Host Survival and Transmission.
1233 Cell 168, 503-516.e12. https://doi.org/10.1016/j.cell.2017.01.006

1234 Rodríguez-Nuevo, A., Torres-Sanchez, A., Duran, J.M., De Guirior, C., Martínez-Zamora, M.A.,
1235 Böke, E., 2022. Oocytes maintain ROS-free mitochondrial metabolism by suppressing
1236 complex I. Nature 607, 756–761. https://doi.org/10.1038/s41586-022-04979-5

1237 Seah, N.E., De Magalhaes Filho, C.D., Petrashen, A.P., Henderson, H.R., Laguer, J., Gonzalez,
1238 J., Dillin, A., Hansen, M., Lapierre, L.R., 2016. Autophagy-mediated longevity is
1239 modulated by lipoprotein biogenesis. Autophagy 12, 261–272.
1240 https://doi.org/10.1080/15548627.2015.1127464

1241 Shao, L.-W., Niu, R., Liu, Y., 2016. Neuropeptide signals cell non-autonomous mitochondrial
1242 unfolded protein response. Cell Res. 26, 1182–1196. https://doi.org/10.1038/cr.2016.118

1243 Shen, K., Pender, C.L., Bar-Ziv, R., Zhang, H., Wickham, K., Willey, E., Durieux, J., Ahmad,
1244 Q., Dillin, A., 2022. Mitochondria as Cellular and Organismal Signaling Hubs. Annu.
1245 Rev. Cell Dev. Biol. 38, annurev-cellbio-120420-015303.
1246 https://doi.org/10.1146/annurev-cellbio-120420-015303

1247 Shi, C., Murphy, C.T., 2023. piRNAs regulate a Hedgehog germline-to-soma pro-aging signal.
1248 Nat. Aging 3, 47–63. https://doi.org/10.1038/s43587-022-00329-2

1249 Shpilka, T., Haynes, C.M., 2018. The mitochondrial UPR: mechanisms, physiological functions
1250 and implications in ageing. Nat. Rev. Mol. Cell Biol. 19, 109–120.
1251 https://doi.org/10.1038/nrm.2017.110

1252 Smith, H.J., Sharma, A., Mair, W.B., 2020. Metabolic Communication and Healthy Aging:
1253 Where Should We Focus Our Energy? Dev. Cell 54, 196–211.
1254 https://doi.org/10.1016/j.devcel.2020.06.011

1255 TeKippe, M., Aballay, A., 2010. C. elegans Germline-Deficient Mutants Respond to Pathogen
1256 Infection Using Shared and Distinct Mechanisms. PLoS ONE 5, e11777.
1257 https://doi.org/10.1371/journal.pone.0011777

1258 The Galaxy Community, Afgan, E., Nekrutenko, A., Grüning, Bjórn A, Blankenberg, D.,
1259 Goecks, J., Schatz, M.C., Ostrovsky, A.E., Mahmoud, A., Lonie, A.J., Syme, A.,
1260 Fouilloux, A., Bretaudeau, A., Nekrutenko, A., Kumar, A., Eschenlauer, A.C., DeSanto,
1261 A.D., Guerler, A., Serrano-Solano, B., Batut, B., Grüning, Björn A, Langhorst, B.W.,
1262 Carr, B., Raubenolt, B.A., Hyde, C.J., Bromhead, C.J., Barnett, C.B., Royaux, C.,
1263 Gallardo, C., Blankenberg, D., Fornika, D.J., Baker, D., Bouvier, D., Clements, D., De
1264 Lima Morais, D.A., Tabernero, D.L., Lariviere, D., Nasr, E., Afgan, E., Zambelli, F.,
1265 Heyl, F., Psomopoulos, F., Coppens, F., Price, G.R., Cuccuru, G., Corguillé, G.L., Von
1266 Kuster, G., Akbulut, G.G., Rasche, H., Hotz, H.-R., Eguinoa, I., Makunin, I., Ranawaka,
1267 I.J., Taylor, J.P., Joshi, J., Hillman-Jackson, J., Goecks, J., Chilton, J.M., Kamali, K.,
1268 Suderman, K., Poterlowicz, K., Yvan, L.B., Lopez-Delisle, L., Sargent, L., Bassetti,
1269 M.E., Tangaro, M.A., Van Den Beek, M., Čech, M., Bernt, M., Fahrner, M., Tekman, M.,
1270 Föll, M.C., Schatz, M.C., Crusoe, M.R., Roncoroni, M., Kucher, N., Coraor, N., Stoler,
1271 N., Rhodes, N., Soranzo, N., Pinter, N., Goonasekera, N.A., Moreno, P.A., Videm, P.,
1272 Melanie, P., Mandreoli, P., Jagtap, P.D., Gu, Q., Weber, R.J.M., Lazarus, R., Vorderman,
1273 R.H.P., Hiltemann, S., Golitsynskiy, S., Garg, S., Bray, S.A., Gladman, S.L., Leo, S.,

1274 Mehta, S.P., Griffin, T.J., Jalili, V., Yves, V., Wen, V., Nagampalli, V.K., Bacon, W.A.,
1275 De Koning, W., Maier, W., Briggs, P.J., 2022. The Galaxy platform for accessible,
1276 reproducible and collaborative biomedical analyses: 2022 update. Nucleic Acids Res. 50,
1277 W345–W351. https://doi.org/10.1093/nar/gkac247

1278 Tsang, W.Y., Lemire, B.D., 2002. Mitochondrial Genome Content Is Regulated during
1279 Nematode Development. Biochem. Biophys. Res. Commun. 291, 8–16.
1280 https://doi.org/10.1006/bbrc.2002.6394

1281 Van Blerkom, J., 2011. Mitochondrial function in the human oocyte and embryo and their role in
1282 developmental competence. Mitochondrion 11, 797–813.
1283 https://doi.org/10.1016/j.mito.2010.09.012

1284 Van Oosten-Hawle, P., 2023. Exploiting inter-tissue stress signaling mechanisms to preserve
1285 organismal proteostasis during aging. Front. Physiol. 14, 1228490.
1286 https://doi.org/10.3389/fphys.2023.1228490

1287 Wang, M.C., O'Rourke, E.J., Ruvkun, G., 2008. Fat Metabolism Links Germline Stem Cells and
1288 Longevity in *C. elegans*. Science 322, 957–960. https://doi.org/10.1126/science.1162011

1289 Watts, J.L., Browse, J., 2002. Genetic dissection of polyunsaturated fatty acid synthesis in
1290 *Caenorhabditis elegans*. Proc. Natl. Acad. Sci. 99, 5854–5859.
1291 https://doi.org/10.1073/pnas.092064799

1292 Whon, T.W., Kim, H.S., Shin, N., Jung, E.S., Tak, E.J., Sung, H., Jung, M., Jeong, Y., Hyun, D.,
1293 Kim, P.S., Jang, Y.K., Lee, C.H., Bae, J., 2021. Male castration increases adiposity via
1294 small intestinal microbial alterations. EMBO Rep. 22, e50663.
1295 https://doi.org/10.15252/embr.202050663

1296 Xin, N., Durieux, J., Yang, C., Wolff, S., Kim, H.-E., Dillin, A., 2022. The UPR ^{mt} Preserves
1297 Mitochondrial Import to Extend Lifespan (preprint). Cell Biology.
1298 https://doi.org/10.1101/2020.07.01.182980

1299 Youle, R.J., Van Der Bliek, A.M., 2012. Mitochondrial Fission, Fusion, and Stress. Science 337,
1300 1062–1065. https://doi.org/10.1126/science.1219855

1301 Zhang, N., Sun, A., Sun, S., Yang, R., Shi, Y., Wang, Q., Li, X., Ma, J., Yue, W., Xie, B., Qiao,
1302 J., Li, M., 2021. Mitochondrial proteome of mouse oocytes and cisplatin-induced shifts in
1303 protein profile. Acta Pharmacol. Sin. 42, 2144–2154. https://doi.org/10.1038/s41401-021-
1304 00687-4

1305 Zhang, Q., Wang, Z., Zhang, W., Wen, Q., Li, X., Zhou, J., Wu, X., Guo, Y., Liu, Y., Wei, C.,
1306 Qian, W., Tian, Y., 2021. The memory of neuronal mitochondrial stress is inherited
1307 transgenerationally via elevated mitochondrial DNA levels. Nat. Cell Biol. 23, 870–880.
1308 https://doi.org/10.1038/s41556-021-00724-8

1309 Zhang, Q., Wu, X., Chen, P., Liu, L., Xin, N., Tian, Y., Dillin, A., 2018. The Mitochondrial
1310 Unfolded Protein Response Is Mediated Cell-Non-autonomously by Retromer-Dependent
1311 Wnt Signaling. Cell 174, 870-883.e17. https://doi.org/10.1016/j.cell.2018.06.029

1312 Zhou, X.-R., Green, A.G., Singh, S.P., 2011. Caenorhabditis elegans Δ12-Desaturase FAT-2 Is a
1313 Bifunctional Desaturase Able to Desaturate a Diverse Range of Fatty Acid Substrates at

1314 the Δ12 and Δ15 Positions. J. Biol. Chem. 286, 43644–43650.
1315 https://doi.org/10.1074/jbc.M111.266114

1316 Zou, L., Wu, D., Zang, X., Wang, Z., Wu, Z., Chen, D., 2019. Construction of a germline-
1317 specific RNAi tool in C. elegans. Sci. Rep. 9, 2354. https://doi.org/10.1038/s41598-019-
1318 38950-8

1319

Figure 1

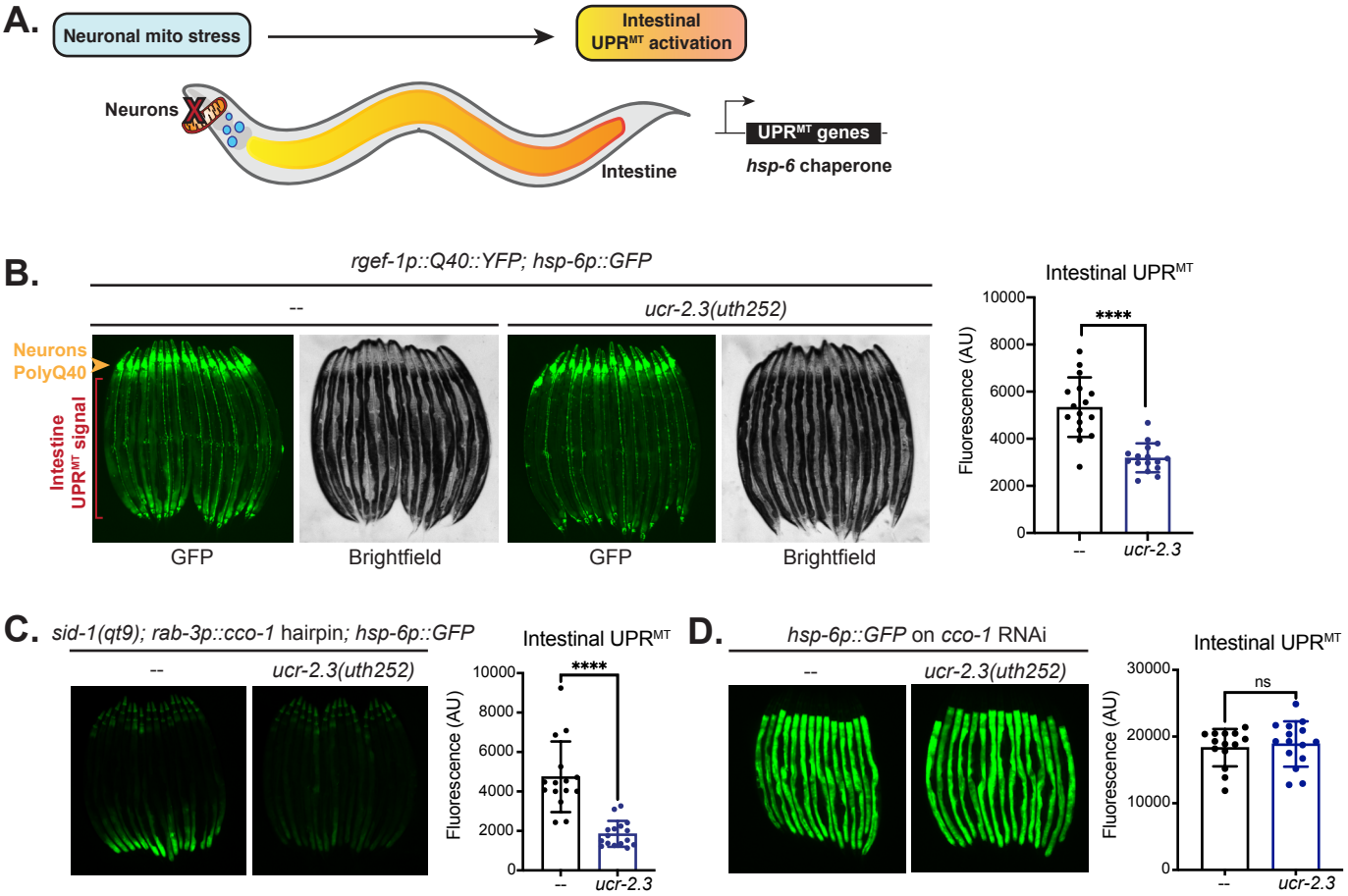
A.
Neuronal mito stress
Intestinal UPR^MT activation
Neurons
Intestine
UPR^MT genes
hsp-6 chaperone
B.
rgef-1p::Q40::YFP; hsp-6p::GFP
--
ucr-2.3(uth252)
Neurons PolyQ40
Intestine UPR^MT signal
GFP
Brightfield
GFP
Brightfield
Intestinal UPR^MT
Fluorescence (AU)
10000
8000
6000
4000
2000
0
****
--
ucr-2.3
C.
sid-1(qt9); rab-3p::cco-1 hairpin; hsp-6p::GFP
--
ucr-2.3(uth252)
Intestinal UPR^MT
Fluorescence (AU)
10000
8000
6000
4000
2000
0
****
--
ucr-2.3
D.
hsp-6p::GFP on cco-1 RNAi
--
ucr-2.3(uth252)
Intestinal UPR^MT
Fluorescence (AU)
30000
20000
10000
0
ns
--
ucr-2.3

Figure 2

A. *i.*

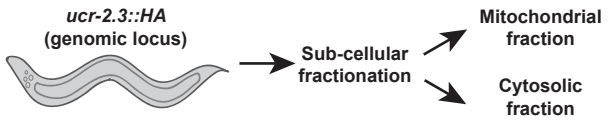

ii.

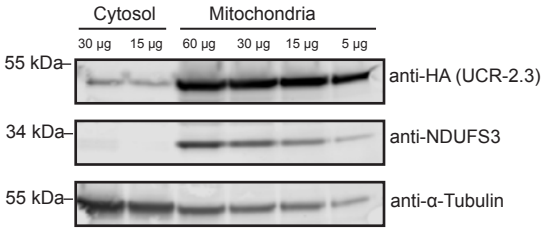

B. *i.*

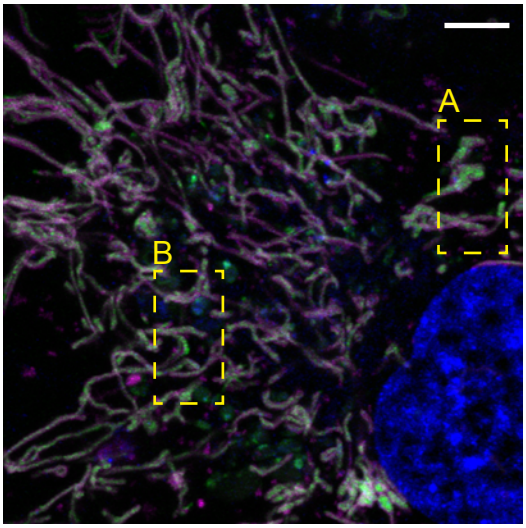

ii.

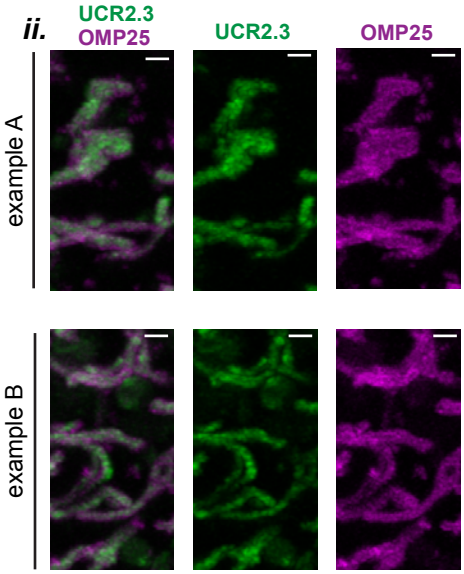

C.

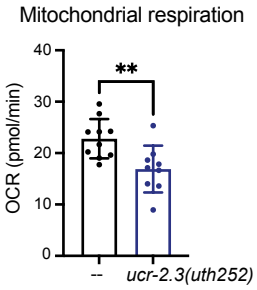

D.

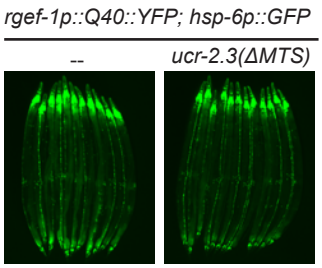

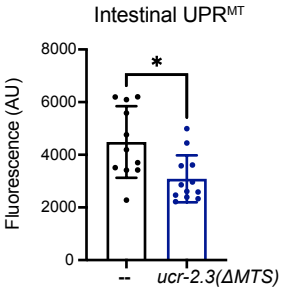

Figure 3

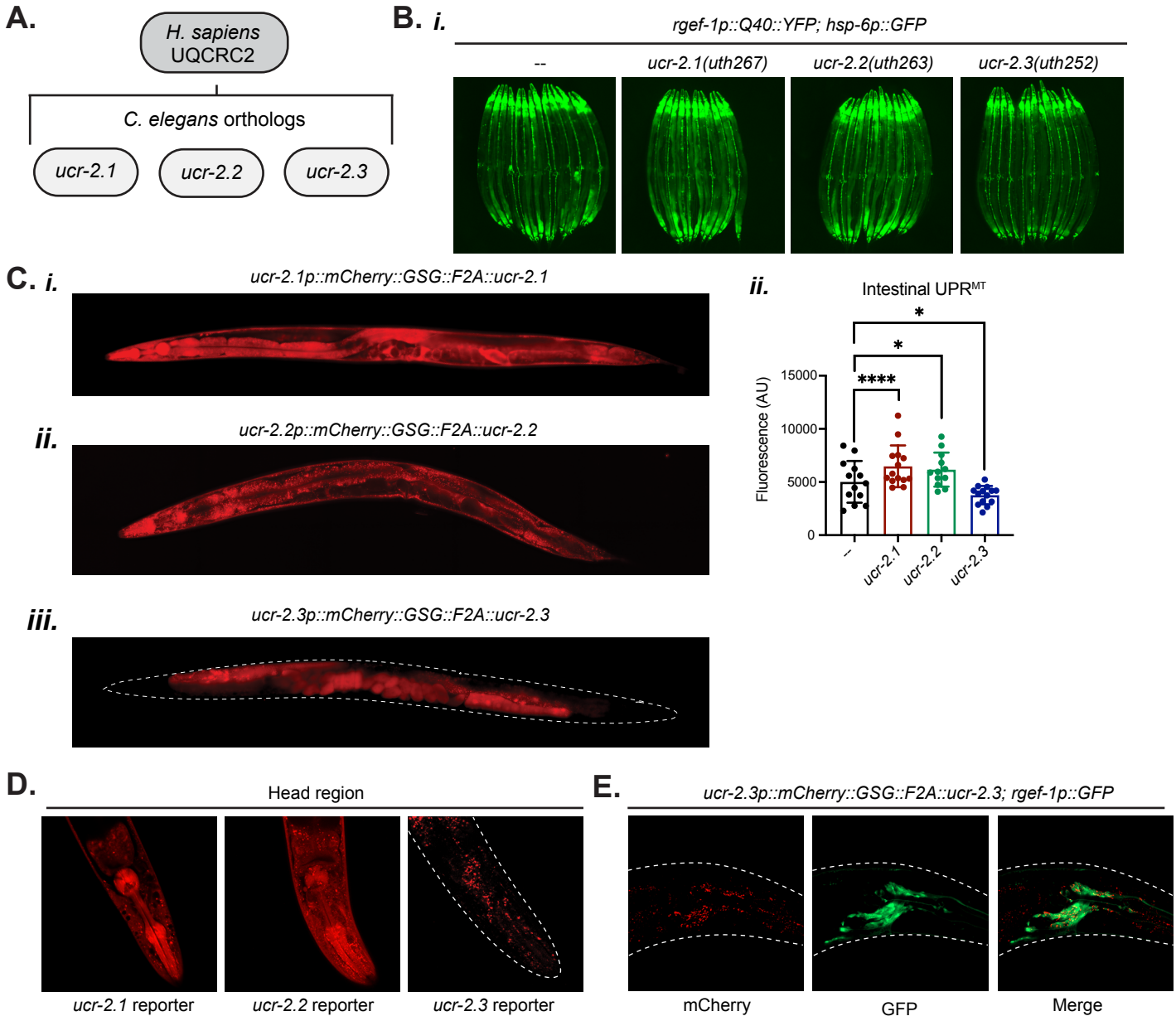
A.
H. sapiens UQCRC2
C. elegans orthologs
ucr-2.1
ucr-2.2
ucr-2.3
B. i.
rgef-1p::Q40::YFP; hsp-6p::GFP
--
ucr-2.1(uth267)
ucr-2.2(uth263)
ucr-2.3(uth252)
C. i.
ucr-2.1p::mCherry::GSG::F2A::ucr-2.1
ii.
ucr-2.2p::mCherry::GSG::F2A::ucr-2.2
iii.
ucr-2.3p::mCherry::GSG::F2A::ucr-2.3
ii.
Intestinal UPRMT
Fluorescence (AU)
15000
10000
5000
0
****
*
*
--
ucr-2.1
ucr-2.2
ucr-2.3
D.
Head region
ucr-2.1 reporter
ucr-2.2 reporter
ucr-2.3 reporter
E.
ucr-2.3p::mCherry::GSG::F2A::ucr-2.3; rgef-1p::GFP
mCherry
GFP
Merge

Figure 4

A. Design of mosSCI tissue-specific rescue experiment:

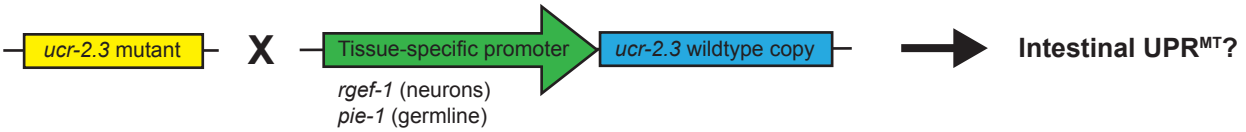

B. i.

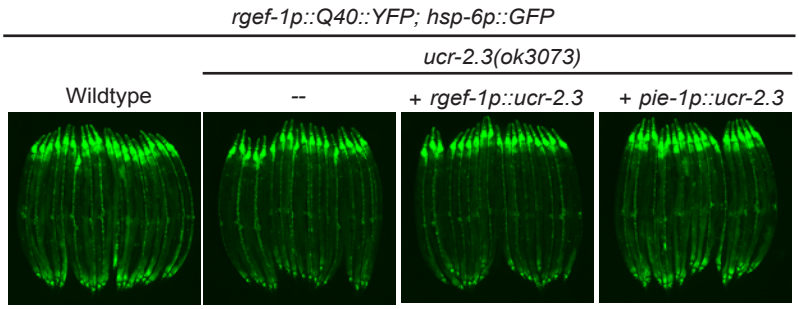

ii.

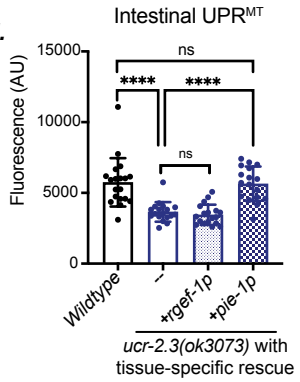

C.

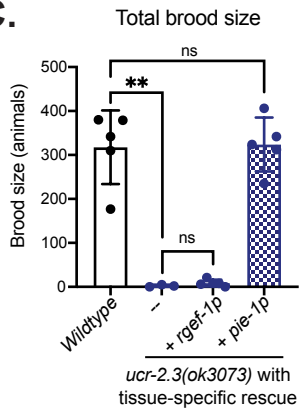

D.

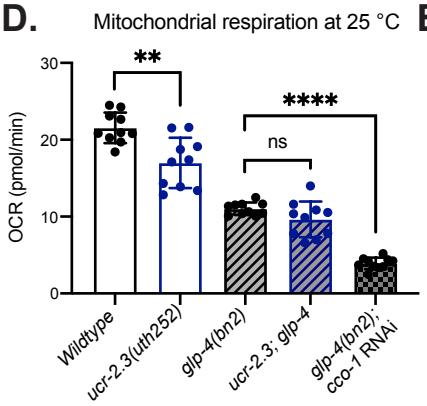

E. i.

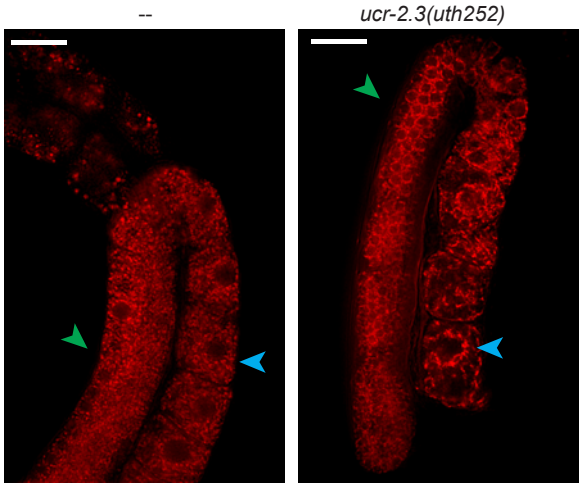

ii.

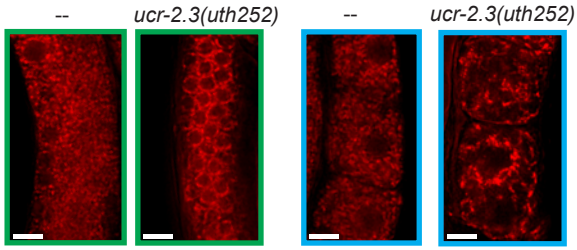

F. i.

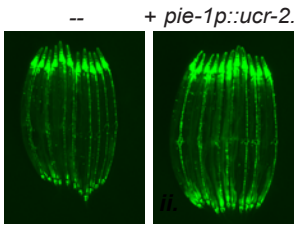

ii.

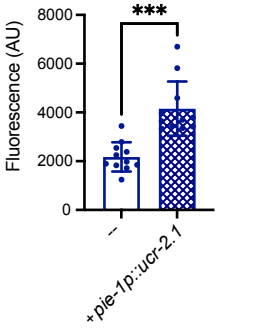

G. i.

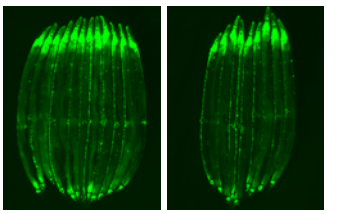

ii.

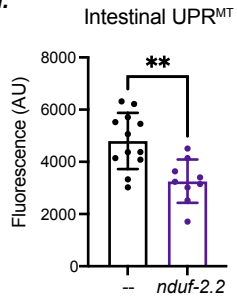

iii.

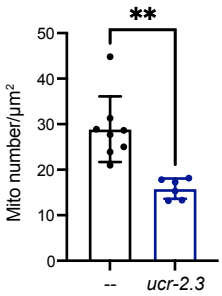

iv.

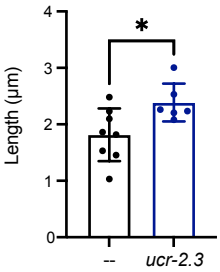

Figure 5

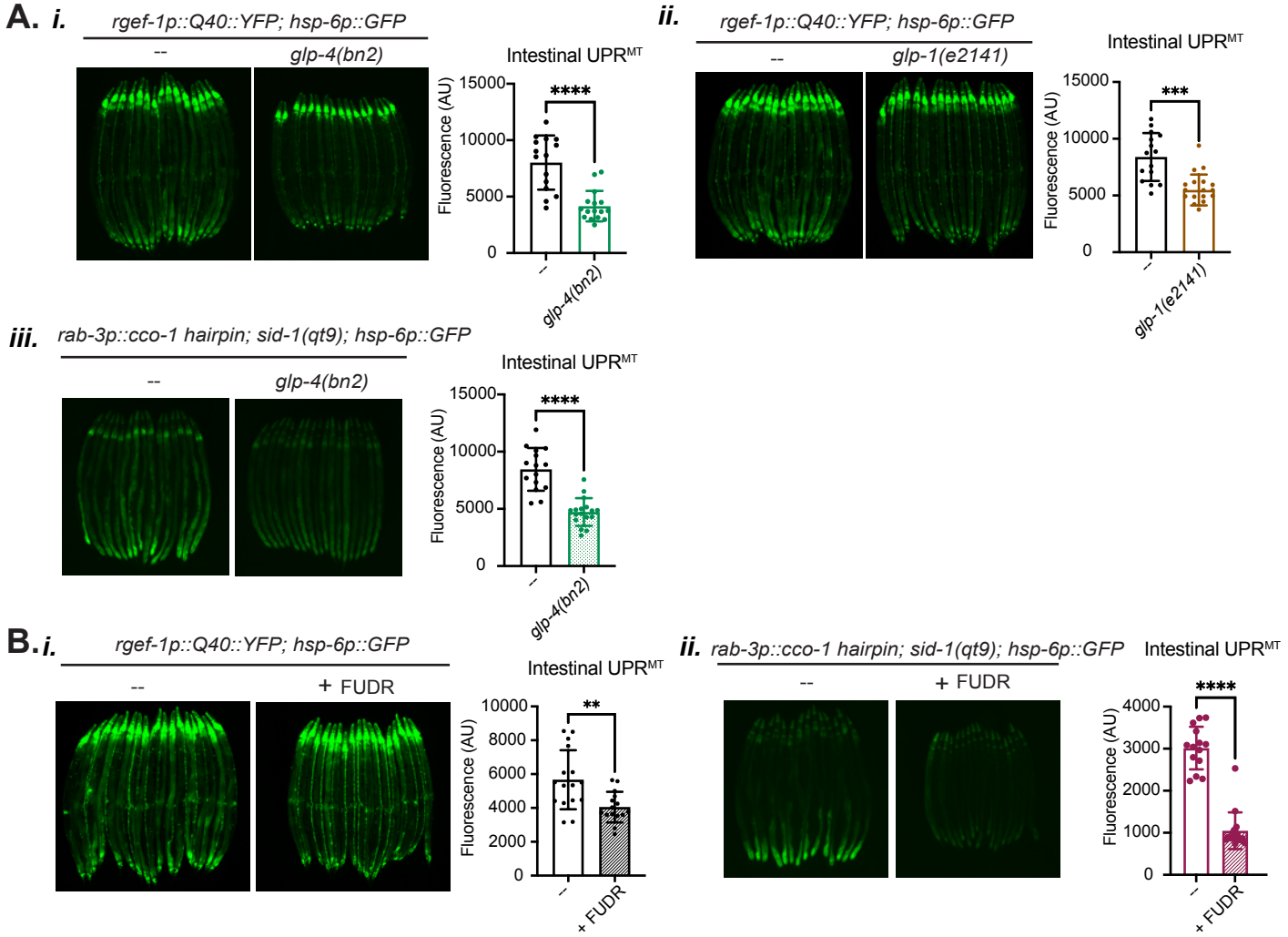
A. i.
rgef-1p::Q40::YFP; hsp-6p::GFP
--
glp-4(bn2)
Intestinal UPRMT
Fluorescence (AU)
15000
10000
5000
0
****
--
glp-4(bn2)
ii.
rgef-1p::Q40::YFP; hsp-6p::GFP
--
glp-1(e2141)
Intestinal UPRMT
Fluorescence (AU)
15000
10000
5000
0
***
--
glp-1(e2141)
iii.
rab-3p::cco-1 hairpin; sid-1(qt9); hsp-6p::GFP
--
glp-4(bn2)
Intestinal UPRMT
Fluorescence (AU)
15000
10000
5000
0
****
--
glp-4(bn2)
B. i.
rgef-1p::Q40::YFP; hsp-6p::GFP
--
+ FUDR
Intestinal UPRMT
Fluorescence (AU)
10000
8000
6000
4000
2000
0
**
--
+ FUDR
ii.
rab-3p::cco-1 hairpin; sid-1(qt9); hsp-6p::GFP
--
+ FUDR
Intestinal UPRMT
Fluorescence (AU)
4000
3000
2000
1000
0
****
--
+ FUDR

Figure 6

A.

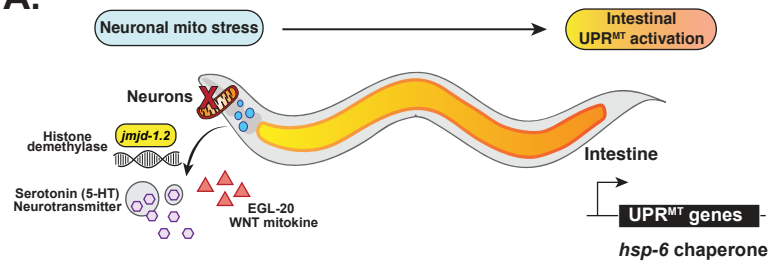

B.

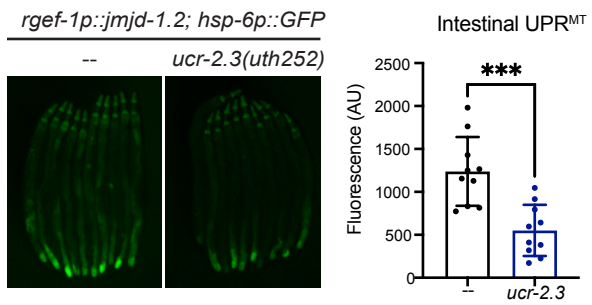

C.

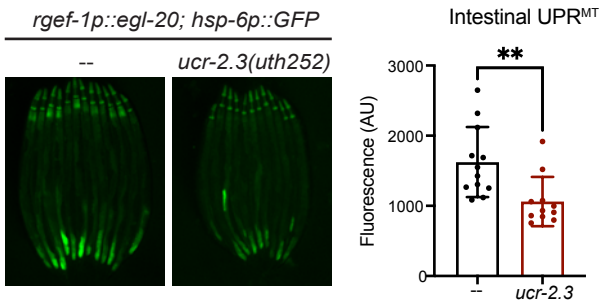

D.

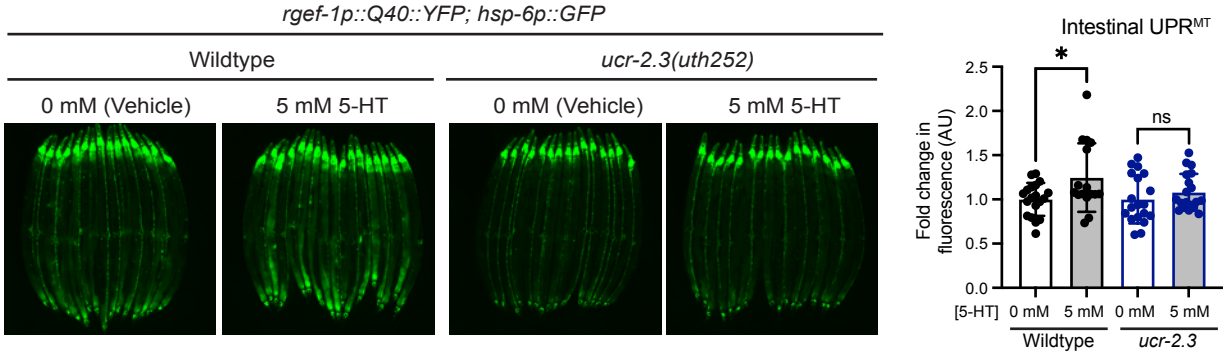

Figure 7

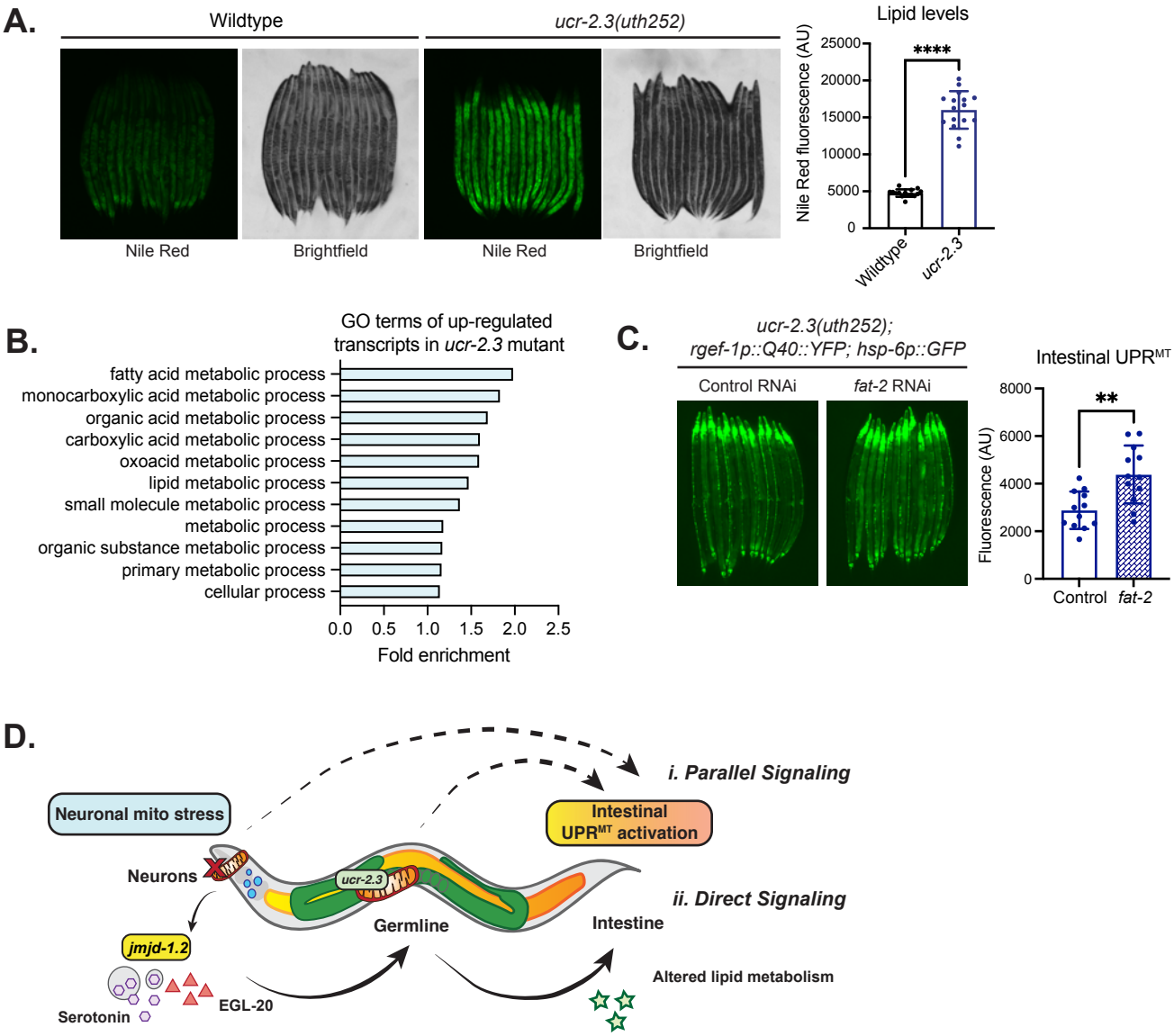
A.
Wildtype
ucr-2.3(uth252)
Nile Red
Brightfield
Nile Red
Brightfield
Lipid levels
Nile Red fluorescence (AU)
25000
20000
15000
10000
5000
0
****
Wildtype
ucr-2.3
B.
GO terms of up-regulated transcripts in ucr-2.3 mutant
fatty acid metabolic process
monocarboxylic acid metabolic process
organic acid metabolic process
carboxylic acid metabolic process
oxoacid metabolic process
lipid metabolic process
small molecule metabolic process
metabolic process
organic substance metabolic process
primary metabolic process
cellular process
0.0
0.5
1.0
1.5
2.0
2.5
Fold enrichment
C.
ucr-2.3(uth252); rgef-1p::Q40::YFP; hsp-6p::GFP
Control RNAi
fat-2 RNAi
Intestinal UPRMT
Fluorescence (AU)
8000
6000
4000
2000
0
**
Control
fat-2
D.
i. Parallel Signaling
Neuronal mito stress
Intestinal UPRMT activation
Neurons
ucr-2.3
ii. Direct Signaling
Germline
Intestine
jmjd-1.2
Serotonin
EGL-20
Altered lipid metabolism

Supplementary Figure 1

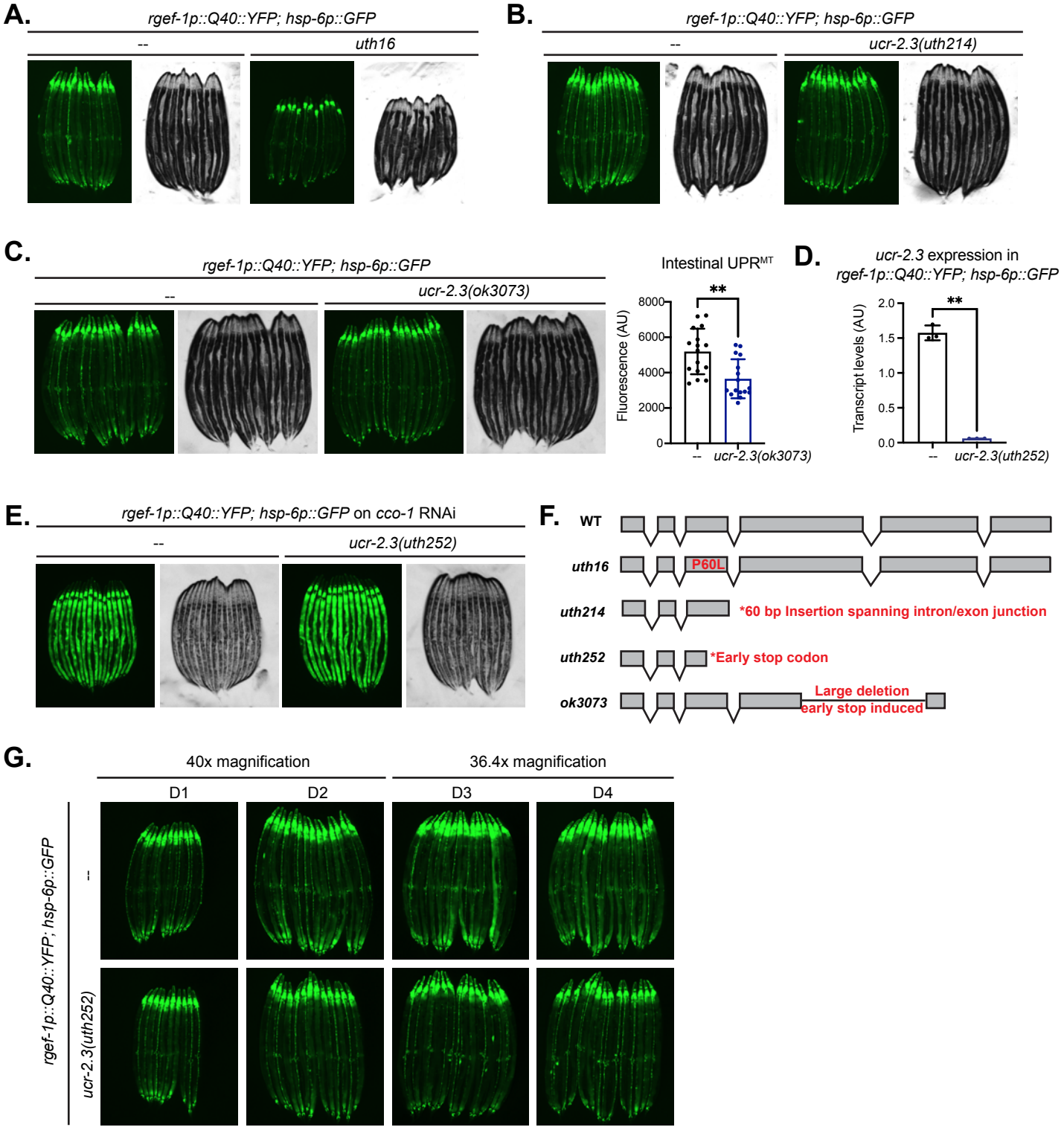

Supplementary Figure 2

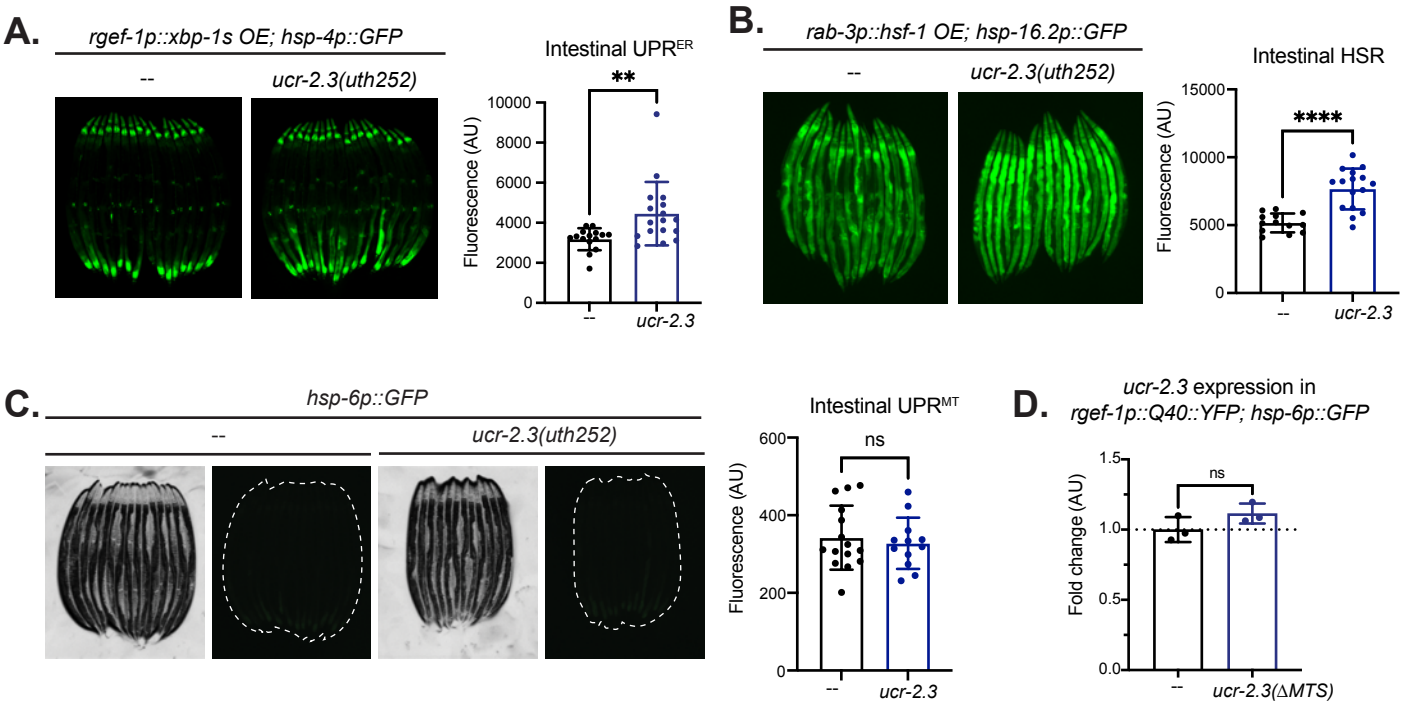

Supplementary Figure 3

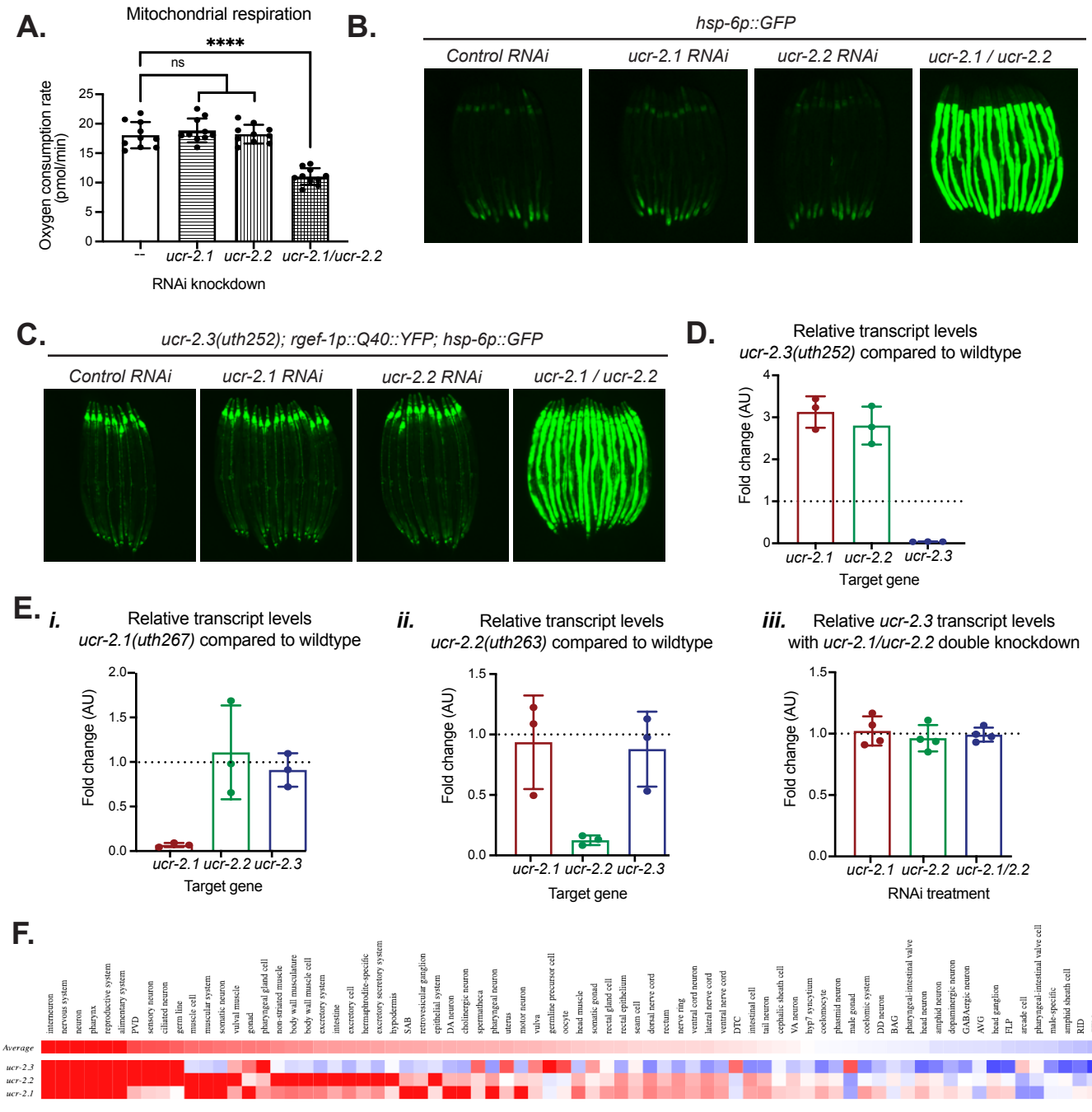

Supplementary Figure 4

A. ***i.***

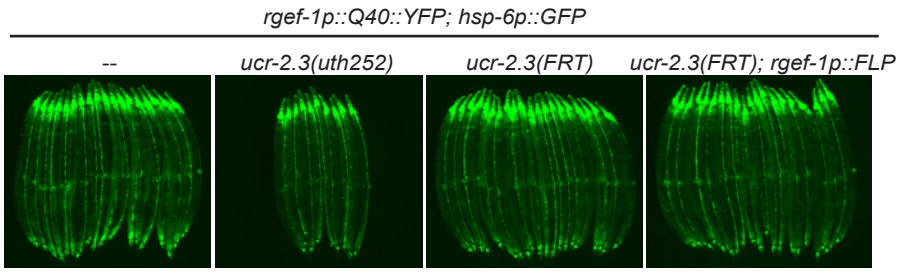

ii.

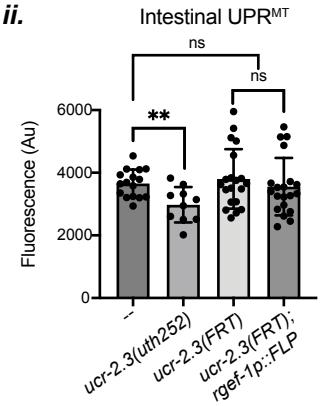

iii.

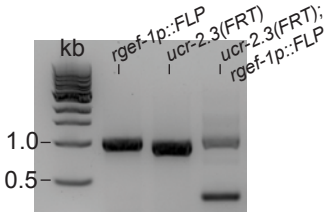

PCR product at *ucr-2.3* genomic locus

B.

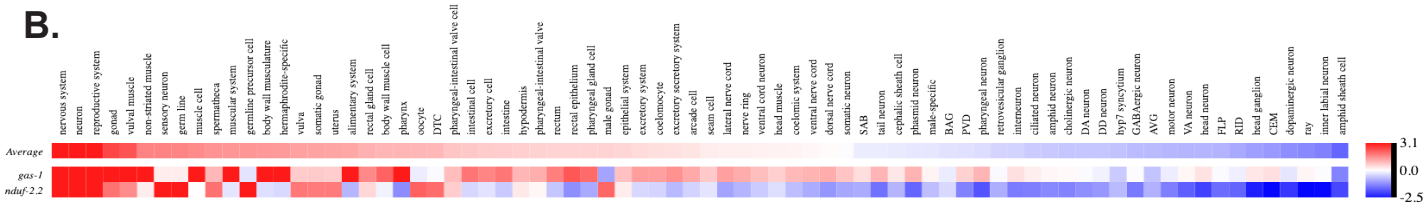

C.

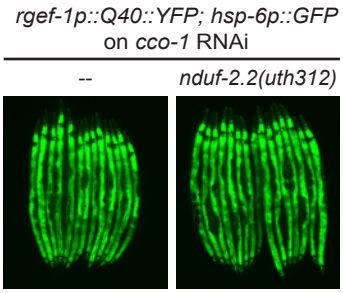

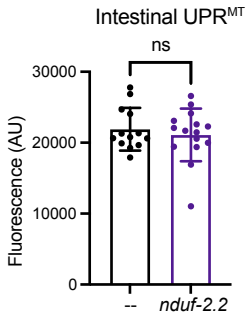

Supplementary Figure 5

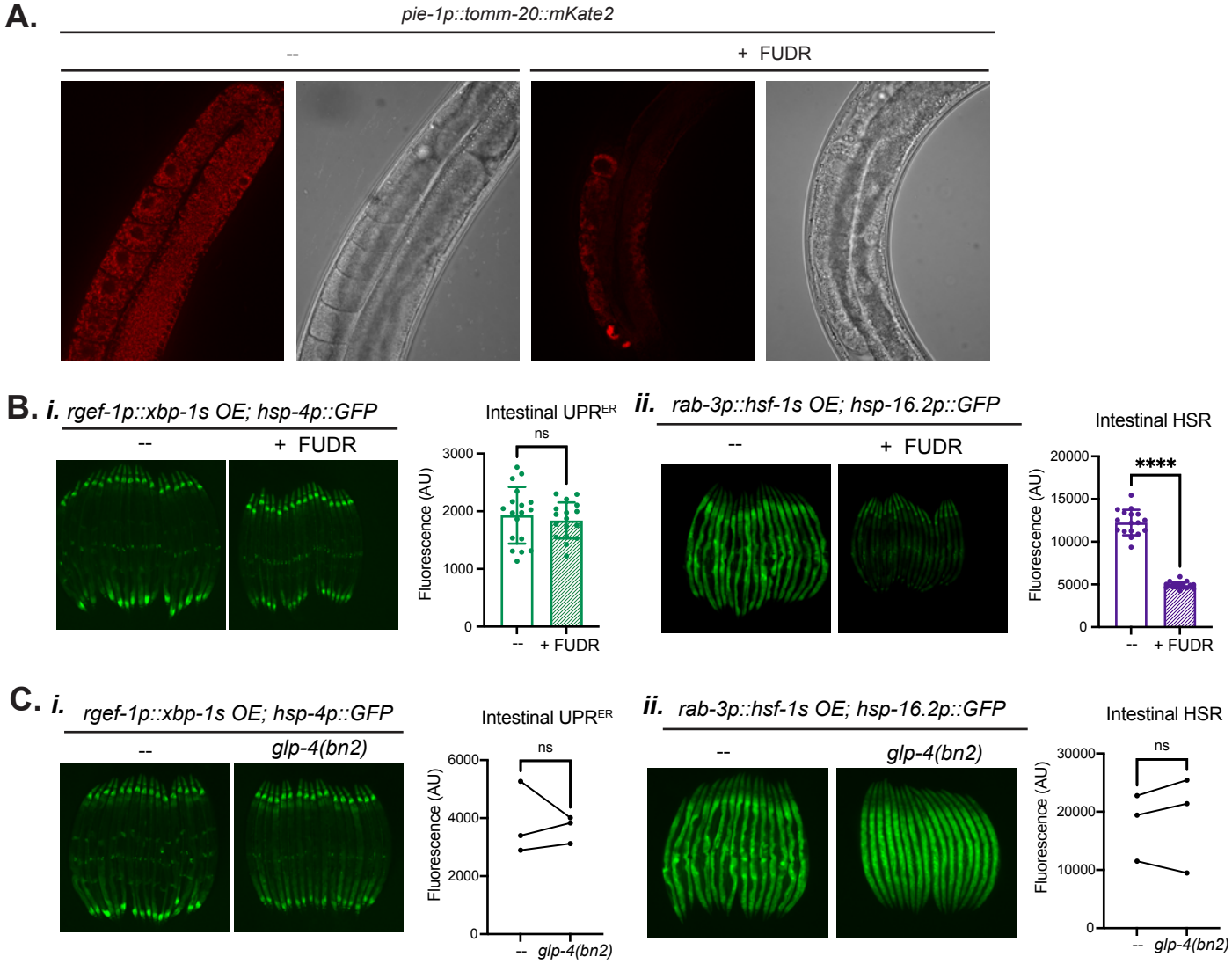

Supplementary Figure 6

A. ***i.*** *sun-1p::rde-1; rde-1(mkc36); rgef-1p::Q40::YFP; hsp-6p::GFP*

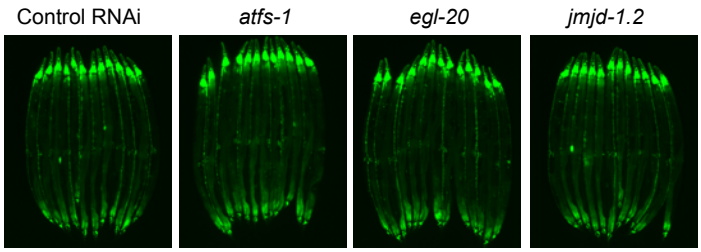

ii. *rgef-1p::Q40::YFP; hsp-6p::GFP*

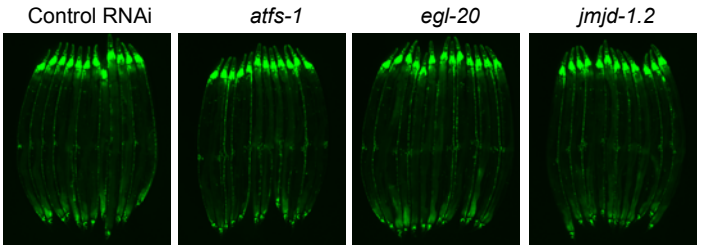
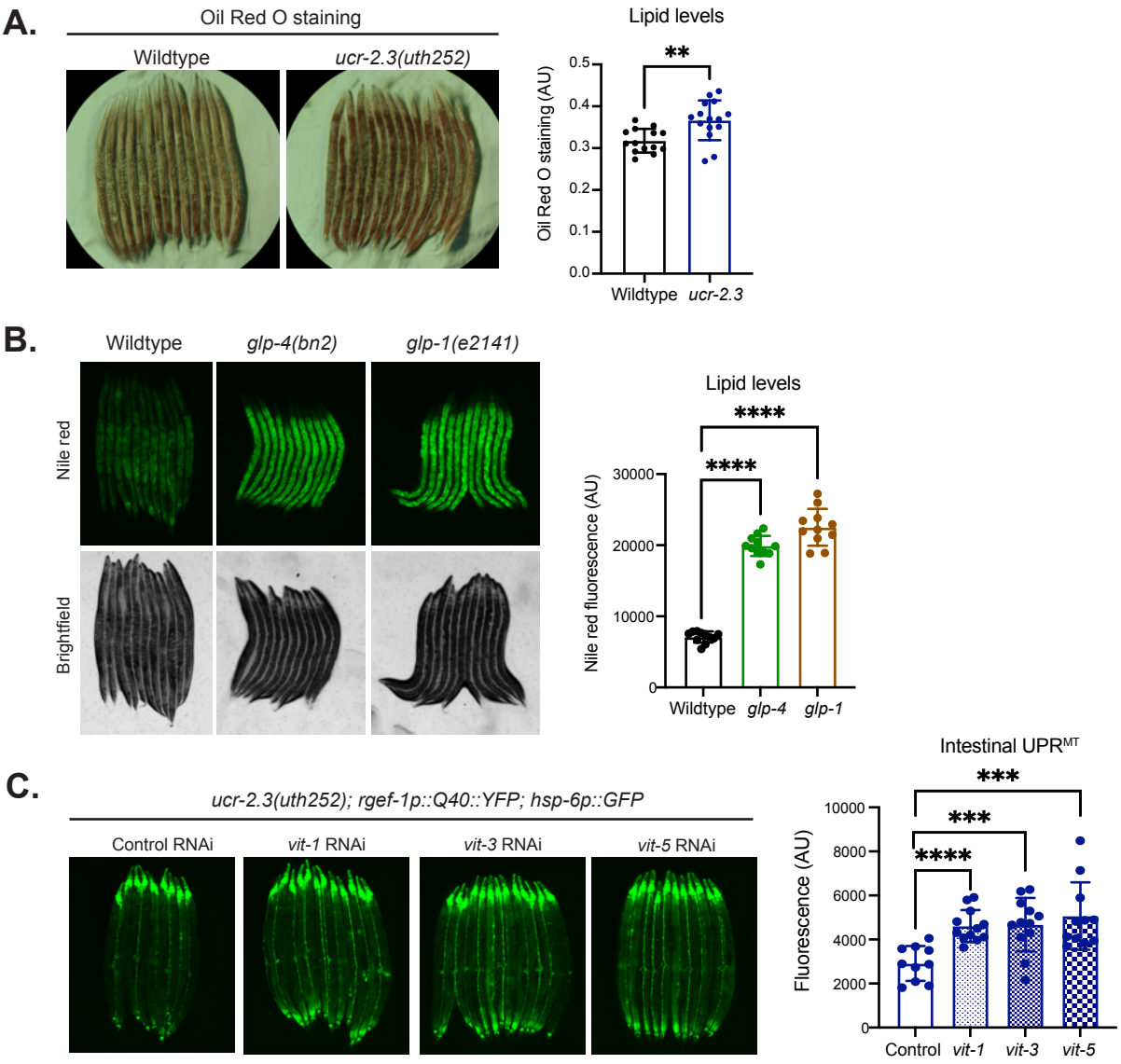
Supplemental Figure 7